GAMMA-RAY SOURCES OBSERVED BY COS-B*

W. HERMSEN

Cosmic-Ray Working Group, Huygens Laboratorium, Leiden, The Netherlands

Abstract. The nature of the fine-scale structure in the gamma-ray distribution is not yet disclosed. Considerable debate is going on whether these structures which appear point-like in the data, are mainly diffuse in nature or are genuinely compact objects. Most of the uncertainty is due to the experimental limitations. A status report is presented on the experimental study of the fine-scale structure measured by COS-B in the energy range 50 MeV–5 GeV. All *identified* gamma-ray sources are discussed: (i) the temporal and spectral characteristics of the radio pulsars PSR053 + 21 and PSR0833–45; (ii) COS-B upper limits on the gamma-ray flux from the binary system Cyg X-3; (iii) the ρ Oph molecular cloud now shown to be resolved in gamma rays as is the case for the Orion complex; (iv) the evidence on the detection of 3C273 in three COS-B observations. The 2CG catalogue of high-energy (point-like) gamma-ray sources contains 25 sources, of which 21 are not yet unambiguously identified. Their average properties are discussed. The error region of the unidentified source 2CG195 + 04 (Geminga) is studied at other wavelengths in greatest detail. This search for a counterpart is summarized, showing the possibility that a nearby ($\lesssim$ 100 pc) neutron star is the counterpart. In the appendix is presented the cross-correlation method which is applied in the search for gamma-ray sources, as well as the appearances of the sources in the data.

1. Introduction

The European Space Agency's satellite COS-B (Bignami *et al.*, 1975; Scarsi *et al.*, 1977) was launched from NASA's Western Test Range on August 9th, 1975. Being switched off on April 25th, 1982, the COS-B gamma-ray experiment, capable of detecting gamma rays with energies greater than $\sim$ 50 MeV, provided 6.7 years of observation time. The total number of useful gamma-ray events is well over 100 000. Since 1976 a large number of publications appeared in print, based on part of the final data base. After the conclusion of the observations a final, more detailed analysis could be started on the different topics addressed in gamma-ray astronomy, taking advantage of the improved counting statistics, of the knowledge gained in gamma-ray astronomy over the last years and of the progress made meanwhile experimentally and theoretically at other wavelengths.

This paper reports on the status of the study of the fine-scale structure in the large-scale gamma-ray distribution before the final digestion of the data. Given the experimental definition of a gamma-ray source, namely, a gamma-ray source is a statistically significant excess above the surrounding background, the excess exhibiting a spatial distribution consistent with the COS-B pointspread function, a search for these sources resulted in the publication of a catalogue of 25 gamma-ray sources using only about $2\frac{1}{2}$ years of data (Swanenburg *et al.*, 1981; Hermsen, 1980, 1981). At the time of compilation of this catalogue in 1979, 1980 no complete surveys were performed yet at mm wavelengths to reveal the clumpy molecular mass distribution (mainly H_2), which, together with the smoother atomic mass distribution (mainly H I) determines pre-

* Proceedings of the XVIII General Assembly of the IAU: *Galactic Astrophysics and Gamma-Ray Astronomy*, held at Patras, Greece, 19 August 1982.

Space Science Reviews **36** (1983) 61–92. 0038–6308/83/0361–0061$04.80.

dominantly the structure of the large-scale, diffuse (i.e. originating from the interaction between cosmic rays and interstellar matter) galactic gamma-ray background. This fact made the search for point sources more difficult. To provide an independent estimate of the diffuse galactic background structure, the new results from radio and mm observations will certainly be used in the final search for gamma-ray sources in the COS-B data. However, the sofar reported gamma-ray sources are present in the data as significant excesses above the surrounding background and have to be explained by whatever feature, object or model. Evidence for their presence is given for several sources. Profiles of all sources are shown by Hermsen (1980).

In the following sections mainly experimental results are presented in view of the long list of papers in this volume adressing searches for counterparts of sofar unidentified gamma-ray sources and theoretical models which try to explain the nature of the gamma-ray sources (identified and unidentified ones). An exhaustive review is given by Bignami and Hermsen (1983). For a more complete account of earlier experimental results see also the latter review.

2. Identified Gamma-Ray Sources

Only a few gamma-ray sources detected in the COS-B energy range (50 MeV–5 GeV) are identified with known astronomical objects, which turned out to be of vastly different nature:

– The radio pulsars PSR 0531 + 21 (Crab pulsar) and PSR 0833 – 45 (Vela pulsar) are unambiguously identified because of their characteristic timing signatures. Both radio-pulsars were already seen in the SAS-2 data (Kniffen *et al.*, 1974; Thompson *et al.*, 1975, respectively), while the Crab pulsar was detected even earlier by instruments flown on balloons (see the review of Fazio, 1973).

– The binary system Cyg X-3 was claimed to be detected at high-energy gamma rays by its characteristic period of ~ 4.8 hr ($E > 40$ MeV, Galper *et al.*, 1976; $E > 35$ MeV, Lamb *et al.*, 1977). However, no confirmation is obtained from the COS-B data (Bennett *et al.*, 1977b; Swanenburg *et al.*, 1981).

– The ρOph molecular cloud was claimed to be seen in the COS-B gamma-ray data (Mayer-Hasselwander *et al.*, 1980; Bignami and Morfill, 1980) because of a spatial coincidence with one of the catalogued gamma-ray sources.

– The quasar 3C 273 is the first (and sofar only) discovered extragalactic high-energy gamma-ray source (Swanenburg *et al.*, 1978). The proposed identification is again based purely on the spatial coincidence with a gamma-ray source.

Results, derived from the COS-B data, on the above mentioned sources are presented concisely in this section.

2.1. Radio pulsars

Vela and Crab. Sofar, gamma-ray emission from radio pulsars has been detected with certainty only from the Vela and Crab pulsars, the only unambiguously identified discrete gamma-ray sources. COS-B had these two sources several times within its field

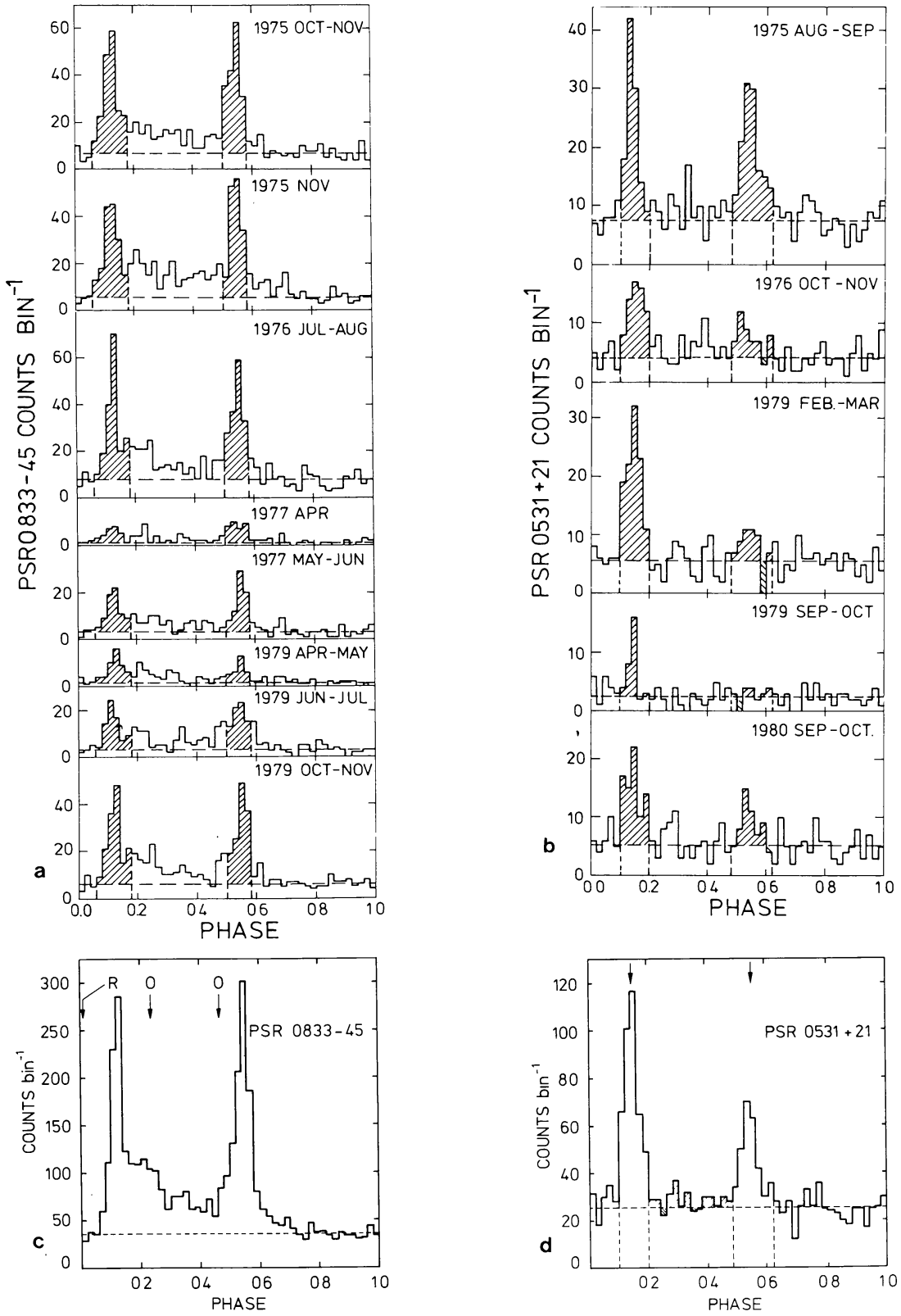

Fig. 1. Gamma-ray light curves of (a) PSR 0833−45 and (b) PSR 0531+21 in the energy interval 50–3000 MeV at the epochs indicated. The shaded areas indicate the phase intervals of the two pulses and the horizontal broken lines show the levels of the background. (c) and (d) present gamma-ray lightcurves obtained by summing the individual curves. PSR 0833−45 (c), the arrows indicate the phases of the radio (R) and optical (O) peaks. PSR 0531+21 (d), the shaded area indicates the interpulse emission and the two arrows indicate the phases of the radio (and optical and X-ray) peaks.

of view, enabling a detailed study of their characteristics in the gamma-ray domain.

Figures 1a and 1b show the phase histograms (light curves) for 8 observations of the Vela pulsar (Wills *et al.*, 1981) resp. 5 observations of the Crab pulsar (Wills *et al.*, 1982) and Figures 1c and 1b present the total (summed) distributions. The similarity of the phase histograms is striking: for both pulsars two peaks are visible with a phase separation of ~ 0.42. At other wavelengths the behaviour of the two pulsars is vastly different: In the case of the Crab, the peakpositions in the optical, X-ray and gamma-ray light curves are coincident to within the timing errors and coincide with the main radiopulse and interpulse (arrows in Figure 1d). Contrary, no pulsed X-ray emission is detected from the Vela pulsar and the pulses in the radio and optical light curves are displaced from the gamma-ray ones (indicated in Figure 1c). Another common feature is the interpulse emission. Averaged over all the observations this amounts to $(15 \pm 4)\%$ of the total pulsed emission from the Crab in the energy range 50 MeV to 3 GeV (Wills *et al.*, 1982; the excess is indicated in Figure 1d), roughly half the percentage in the Vela situation. The Vela light curve not only shows pulsed emission between the two peaks, but also exhibits a tail of pulsed emission after the second peak (Kanbach *et al.*, 1980).

Comparison of Figures 1a and 1b reveals another difference in the behaviour of the two pulsars: The relative strength of the two pulses is constant in the case of the Vela pulsar (Wills *et al.*, 1981) and changed in time in the Crab situation (Wills *et al.*, 1982). This is illustrated in Figure 2.

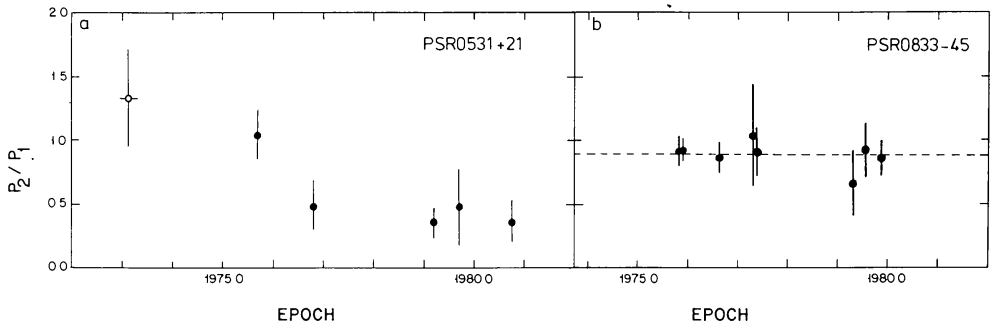

Fig. 2. Variation with time of the ratio of the number of pulsed counts in the second pulse (P2) and the first pulse (P1) of PSR 0531 + 21 (a) and PSR 0833 – 45 (b): open circle, > 35 MeV from SAS-2 data; closed circles, 50–3000 MeV from COS-B data. The broken line in (b) indicates the weighted average of the data points in the Vela case.

The spectral characteristics can be summarized as follows:

– *Vela.* The energy spectra of the different components of the Vela light curve are found to differ significantly. The first pulse exhibits a softer spectrum than the inter-region emission and the second pulse (Kanbach *et al.*, 1980). The shape of the spectrum of the total pulsed emission in the energy range 50 MeV to 3.2 GeV can be represented by a single power law of index 1.89 ± 0.06, with indications of a spectral flattening at low energies and a steepening above a few hundred MeV (Kanbach *et al.*, 1980). The energy spectrum of the total excess at the position of the Vela pulsar is consistent (in flux and shape) with that of the pulsed radiation (Lichti *et al.*, 1980; Hermsen, 1980), indicating that no steady component has been measured.

– *Crab*. No differences in shape are detected sofar between the energy spectra of the emission in the two pulses in the energy range above 50 MeV (Bennett *et al.*, 1977a, using only one observation). The total pulsed spectrum in the energy range 50 MeV to 1 GeV can be represented by a single power law index 2.2 ± 0.2. The total Crab spectrum shows emission in addition to the pulsed component up to energies of about 400 MeV (Lichti *et al.*, 1980; Hermsen 1980).

The total energy spectrum from the radio up to the ultra-high-energy gamma-ray range is presented for the cases of Vela and Crab in Figures 3a and 3b, respectively (from

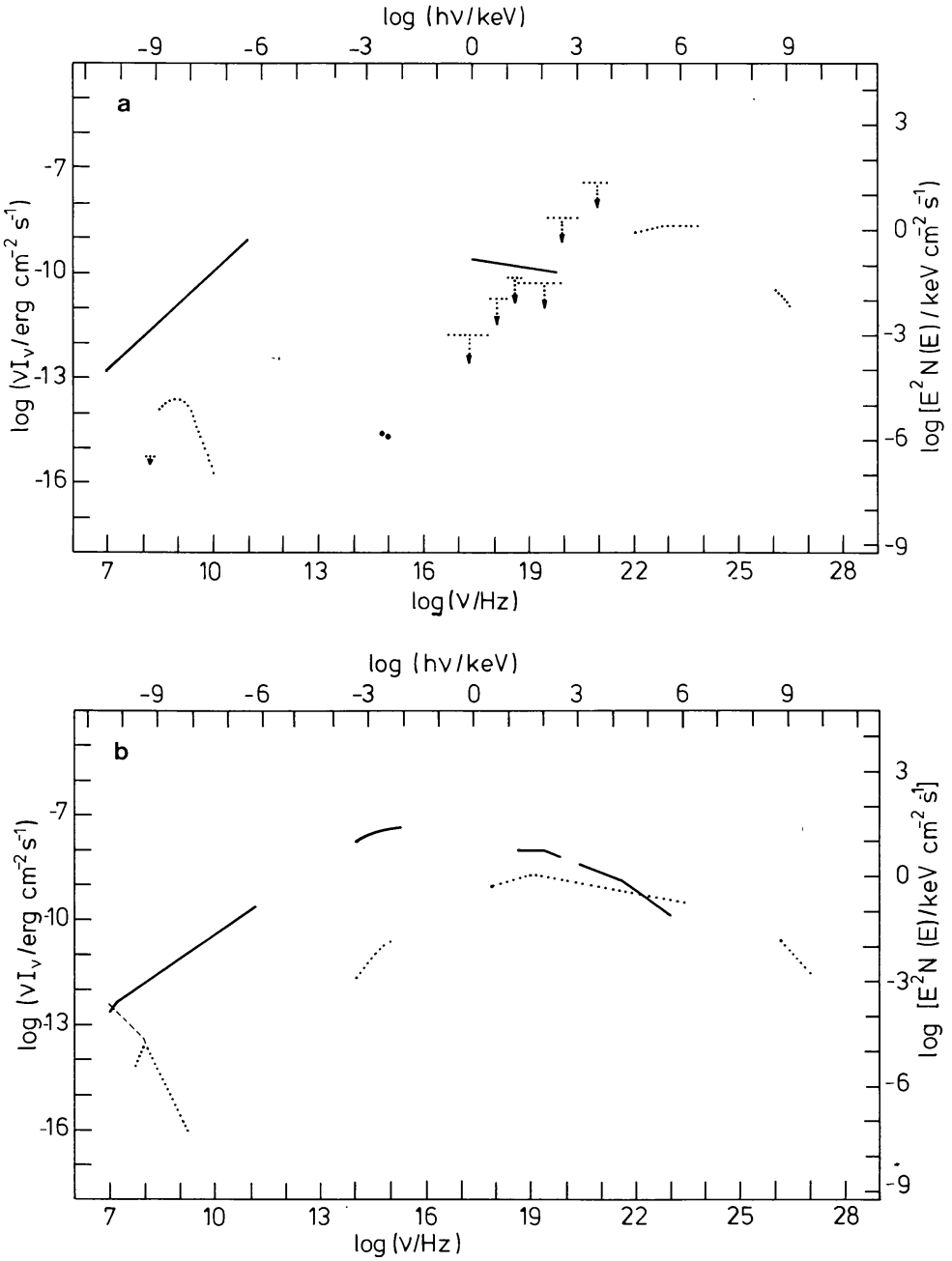

Fig. 3. Distributions of emitted power as a function of frequency for (a) Vela and (b) Crab: Nebula (solid lines), pulsar (dotted lines), compact source (broken line). The data for $E > 500$ GeV are somewhat disputed and show time variability. For data origins see Bignami and Hermsen (1983).

Bignami and Hermsen, 1983). The maximum power of the Vela pulsar is emitted at gamma-ray energies of ~ 1 GeV. The Crab pulsar emits most of its energy in the range of the hard X-rays to the soft gamma rays.

Finally, it is not possible to calculate the intrinsic luminosity of the pulsars exactly, since it depends on the pulsar's beaming geometry; using a conic beam geometry Buccheri (1981) derives for Vela L(50 MeV–10 GeV) $\simeq 4 \times 10^{34}$ erg s^{-1} or a conversion efficiency of $\sim 6 \times 10^{-3}$ and for Crab L(50 MeV–10 GeV) $\simeq 2 \times 10^{35}$ erg s^{-1} or a conversion efficiency of $\sim 4 \times 10^{-4}$.

Other Radio Pulsars. Although a small number of other radio pulsars were reported to emit gamma rays in the COS-B energy range, all the reported effects needed confirmation and none is confirmed. Meanwhile, new radio parameters became available. Of the 330 radio pulsars published in the catalogue of Manchester and Taylor (1981), 117 have parameters measured in time intervals covering 21 COS-B observations. These objects (17 of which have been observed more than once, bringing the total number of independent pulsar observations to 145) have been searched for gamma-ray emission above 50 MeV. Buccheri (1983) presents the results, which were negative in all cases. A 3σ upper limit is therefore calculated for the average gamma-ray flux from these pulsars into gamma rays. This upper limit is 1.2×10^{-7} ph cm^{-2} s^{-1} ($E > 50$ MeV) for pulsed radiation with a gamma-ray light curve similar to that of the Crab and Vela pulsars, implying less than 23% average conversion efficiency (see also Buccheri *et al.*, 1983).

2.2. Cyg X-3

After the great radio outburst in September 1972 (Gregory *et al.*, 1972) and the detection of a periodical variation of ~ 4.8 hr in the X-ray emission (Parsignault *et al.*, 1972), extensive observations of Cyg X-3 have been performed over a wide range of frequencies from the radio range up to the ultra-high-energy gamma rays. For a detailed discussion of the experimental results from the energy domain of the hard X-rays up to $E \geq 10^{16}$ eV, see Bignami and Hermsen (1983) and the summary in Figure 4.

COS-B had the source within its field of view at an inclination angle $< 10°$ during 7 observation periods, each typically of one month duration. A temporal analysis of the data acquired during the first 5 of these observation periods (between November 1975 and November 1980) is carried out. The timing parameters derived from the X-ray data collected with the X-ray detector aboard COS-B (van der Klis and Bonnet-Bidaud, 1981) have been used. Evidence for pulsed gamma-ray emission (at the 4.8 hr periodical variation) is found neither in the data from each individual observation, nor in the combined data set. As a preliminary result a 2σ upper limit to the pulsed flux is calculated for the combined data set. Assuming that the shape of the X-ray phase histogram is expected in the gamma-ray domain, this limit is 2.1×10^{-6} photon cm^{-2} s^{-1} in the energy range 50 MeV to 150 MeV and 0.65×10^{-6} photon cm^{-2} s^{-1} for energies above 150 MeV.

The integral energy spectrum, as summarized by Samorski and Stamm (1983), is given in Figure 4 together with the COS-B 2σ integral upper limits. At present it seems

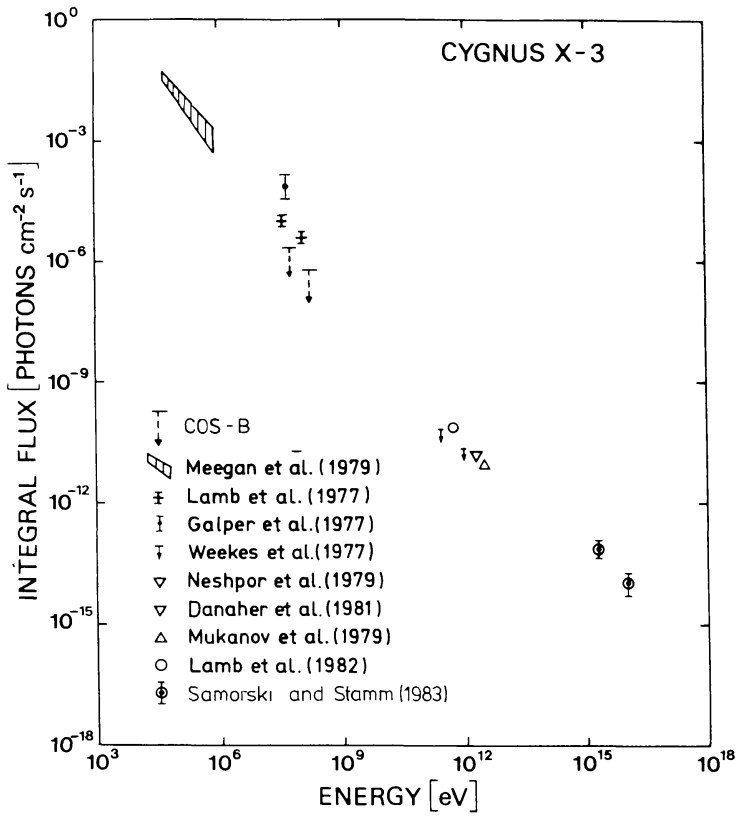

Fig. 4. Integral gamma-ray spectrum of Cygnus X-3 (after Samorski and Stamm, 1983). The flux values are averaged over the total phase. The COS-B upper limits are included as well to show the experimental uncertainties for energies of ~ 100 MeV.

to be firm that the source is detected at ultra-high gamma-ray energies, while the detection at energies around 100 MeV is uncertain, but, if true, would indicate the presence of an extremely variable strong source, reaching a luminosity of $\gtrsim 10^{37}$ erg s^{-1} for a distance of ~ 11 kpc (Lamb *et al.*, 1977). In this context it is worth noting, that the data point in Figure 4 from Galper *et al.* (1977) is the average value over several years, while the measured flux in 1972 was claimed to be as high as 2×10^{-4} photon cm^{-2} s^{-1} ($E > 40$ MeV), or about an order of magnitude higher than the values claimed by the SAS-2 team.

2.3. Molecular clouds

Interstellar clouds can become visible as gamma-ray sources by interaction of cosmic rays and the matter of the clouds, as was first clearly stated by Black and Fazio (1973). Since the gamma-ray source 2CG 353 + 16 (Swanenburg *et al.*, 1981) is located in the direction of the ρOph cloud, identification of this source with ρOph was evidently suggested (Mayer-Hasselwander *et al.*, 1980; Bignami and Morfill, 1980). As a result of improved statistics relative to the database of Swanenburg *et al.* (1981), the source is now spatially resolved, making the identification definite. The ρOph region of the sky is given in Figure 5 (from Hermsen and Bloemen, 1983): Figure 5a shows the gamma-ray map, presenting evidence for resolved structure in gamma rays, and Figure 5b

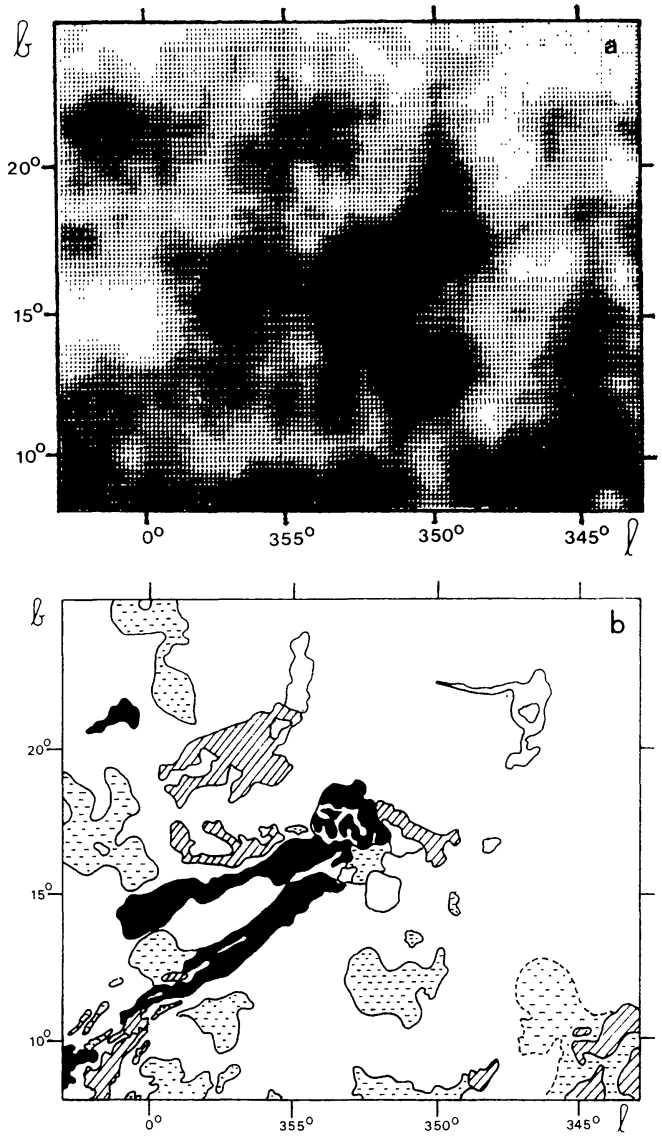

Fig. 5. The ρOph region: (a) half-tone map showing the gamma-ray intensities (100 MeV $< E <$ 5 GeV); (b) sketch from the atlas of dark clouds by Khavtassi (1960). The dotted, shaded and black regions indicate increasing obscuration. The blank features represent bright diffuse nebulae. For a detailed description of the distances of the dark clouds and the molecular gas connected to them see Wouterloot (1981) and references therein. (Figure from Hermsen and Bloemen, 1983.)

presents the distribution of extinction after Khavtassi (1960). The detailed positional correlation is striking, even though the gamma-ray map is measured with appreciably lower resolution. Wouterloot (1981) calculated from his OH measurements a higher mass estimate for the 'upper stream' than for the lower one, both clearly visible in the Khavtassi map (Figure 5b). This is consistent with the measured relative gamma-ray fluxes. A preliminary comparison of the total gamma-ray flux with the rather high mass estimates of Wouterloot (1981), indicates that the gamma-ray flux is within a factor 2 consistent with the gamma-rays being produced by the interaction of cosmic rays with a density equal to that observed in the solar neighbourhood and the estimated total mass (Hermsen and Bloemen, 1983).

The ρOph cloud complex falls now in the same category as the Orion cloud complex, namely a molecular cloud spatially resolved in the COS-B maps. In the case of Orion, the counting statistics obtained during one single observation were sufficient to resolve the structure (Caraveo *et al.*, 1980, 1981). Figure 6 gives a comparison of the gamma-ray map of the Orion region (Figure 6a) and the main part of the complex as seen in CO millimeter emission (Figure 6b). The gamma-ray map includes additional data (compared to Caraveo *et al.*, 1980, 1981) from several observations overlapping partly the Orion complex. The detailed positional correlation is evident, like in the case of ρOph.

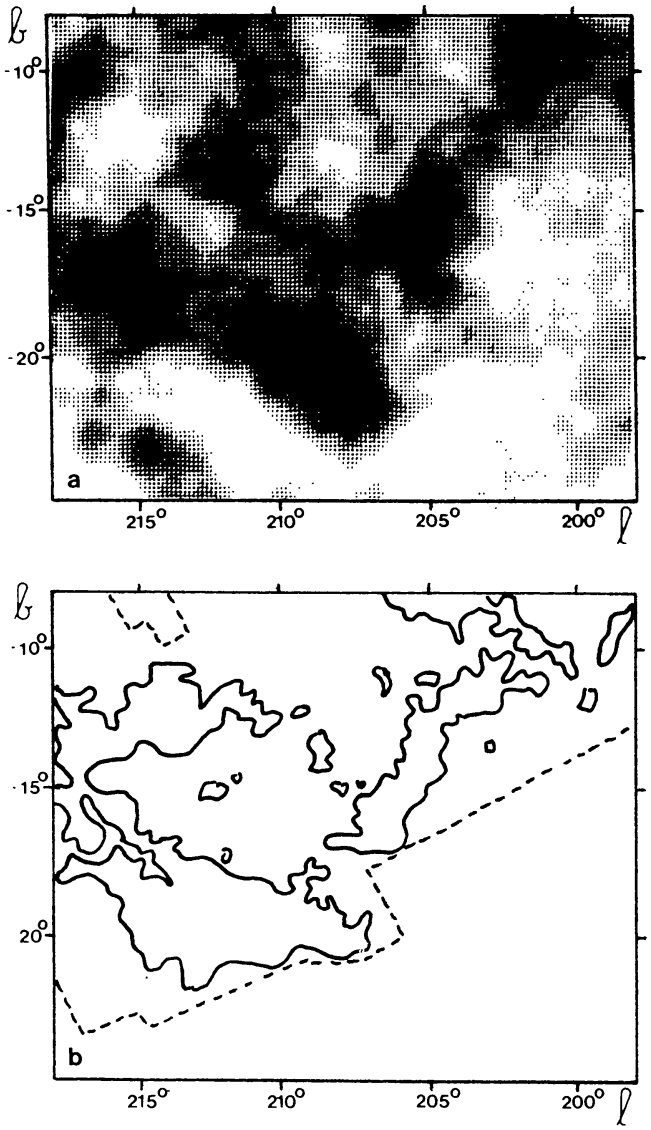

Fig. 6. The Orion region: (a) half-tone map showing the gamma-ray intensities (100 MeV $< E <$ 5 GeV); (b) CO contour plot of 1 K peak antenna temperature (Morris and Thaddeus). (Figure from Bloemen, 1983.)

The total mass of the Orion complex is determined from the gamma-ray data, assuming that the cosmic-ray density at the complex is equal to the local value, and is found to be well in agreement with radio-astronomical estimates (Caraveo *et al.*, 1980, 1981).

2.4. 3C273

COS-B observed the Virgo region of the sky three times. An observation in May, June 1976 led to the discovery of the high-energy (>50 MeV) gamma-ray source CG 291 + 65, which prompted Swanenburg *et al.* (1978) to propose its identification with the quasar 3C273 ($<1\%$ probability of chance coincidence of the gamma-ray source with the specific object 3C273). The second measurement (June, July 1978) confirmed the high-energy gamma-ray emission (Bignami *et al.*, 1981) and the position was updated (2CG 289 + 64; Swanenburg *et al.*, 1981). Finally, Hermsen *et al.* (1981) reported on a third detection, namely from data collected in June, July 1980.

Figure 7 presents the combined evidence for the detection of 3C273 for energies above 100 MeV. The measured arrival directions of the gamma rays of all three observations were sorted into $0.5° \times 0.5°$ bins. The resulting skymap was analyzed using the cross-correlation method described by Hermsen (1980) (see also the appendix). The skymap shown in Figure 7 gives for each bin the number of counts that correlate with the PSF.

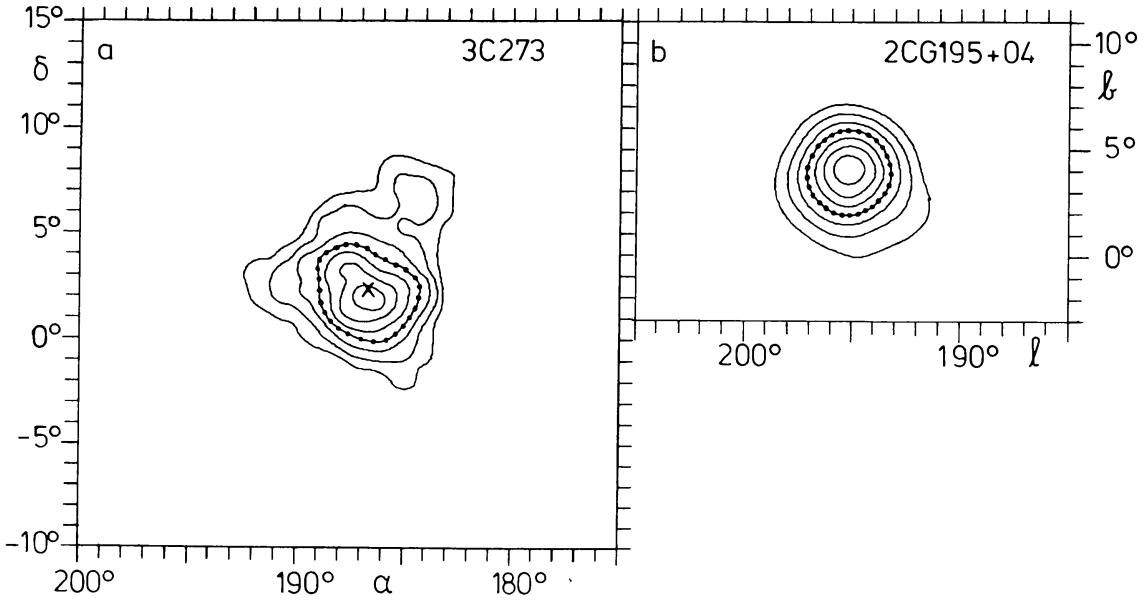

Fig. 7. (a) Contour plot of the correlation map ($E > 100$ MeV) of an area of the sky containing 3C273. The contour levels are indicated at 20, 30, 40, 50, 60, 70, 80 correlated counts. The cross indicates the position of 3C273. (b) For comparison, the strong unidentified gamma-ray source 2CG195 + 04 is shown in the same representation. Contour levels are indicated at 125, 200, 275, 350, 425, 500, 575 correlated counts. The dotted contours indicate for both figures a level of $\sim 56\%$ of the peak values.

In other words, in each bin is given the number of counts that can be attributed to a point source located in that bin. For comparison, the appearance of a point-like gamma-ray source is shown as well, for the same energy range and applying the same cross-correlation analysis. Used is data from the strongest ($E > 100$ MeV), unidentified gamma-ray source, 2CG 195 + 04 (often referred to as Geminga). The gamma-ray source feature at the position of 3C273 contains ~ 90 counts (a confidence level of $8.2\sigma_0$) in a statistically empty (<20 correlated counts) field. The Geminga feature contains ~ 620 counts and reaches a significance of $32.5\sigma_0$. For these high numbers of photon counts σ_0 can be considered to follow Gaussian statistics.

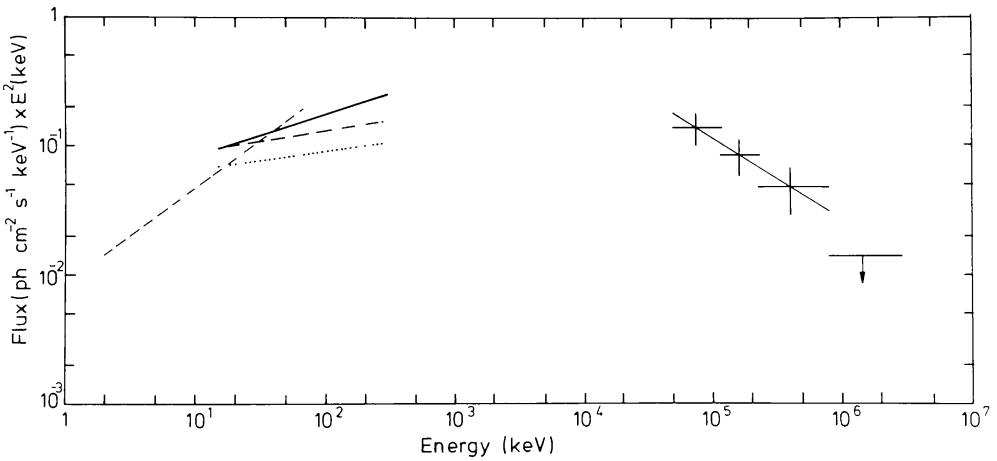

Fig. 8. High-energy spectrum of 3C273 including data from HEAO-1, experiment A2 (broken line), experiment A4 (solid line), the MIT/Leiden balloon experiment, 1979 (broken, dotted line) and 1980 (dotted line) and the COS-B data points with the best fit between 50 and 800 MeV. For references, see Hermsen *et al.* (1981).

The total energy spectrum from the soft X-rays up to the high-energy gamma rays is given in Figure 8 (from Hermsen *et al.*, 1981). Between 50 MeV and 800 MeV the spectrum can be well fitted by the power law:

$$dN/dE = (3.9 \pm 1.2) \times 10^{-6} [E(\mathrm{GeV})/0.15]^{-2.6 \pm 0.4} \text{ photon cm}^{-2}\,\mathrm{s}^{-1}\,\mathrm{GeV}^{-1}\,.$$

The data suggest that the peak luminosity of 3C273 could be expected in the 1 MeV to 10 MeV range. Neither the problem to decide on an appropriate gamma-ray production model, nor that to decide on the location of production in the QSO are sofar solved (see for example the discussion in Bignami *et al.*, 1981).

3. Unidentified Gamma-Ray Sources

3.1. The 2CG catalogue of gamma-ray sources

The Caravane Collaboration published in 1977 the first CG Catalogue of high-energy gamma-ray sources (Hermsen *et al.*, 1977a), which contained 13 sources for a $\sim 40\%$ coverage of the galactic disc. The list of sources was the result from a search following a relatively simple procedure (Hermsen *et al.*, 1977b). This first success stimulated the development of a more sensitive and firm analysis procedure, based on a cross-correlation method, which was presented in full detail by Hermsen (1980). In this method the measured distribution of the photon arrival directions is correlated with the distribution expected for a point source. This latter distribution, the intrinsic point-spread function of the instrument, was determined by pre-launch calibration and confirmed by the actual flight data for the strong Vela gamma-ray source. A gamma-ray source is thus defined as a significant excess which has a spatial distribution consistent with the point-spread function. In an appendix, added to this paper, an extended abstract is presented, which

1983SSRv...36...61H

TABLE I

The 2CG catalogue of gamma-ray sources

Source name	No. of observations	Position		Error radius	Flux[a] $E > 100$ MeV (10^{-6} photons $cm^{-2} s^{-1}$)	Spectral[b] parameter	Comments	CG source (Hermsen *et al.*, 1977)	Identification
		l	b						
2CG 006 – 00	3	6°.7	−0°.5	1°.0	2°.4	0.39 ± 0.08		–	–
2CG 010 – 31	1	10°.5	−31°.5	1°.5	1°.2	–		–	–
2CG 013 + 00	4	13°.7	+0°.6	1°.0	1°.0	0.68 ± 0.14		–	–
2CG 036 + 01	3	36°.5	+1°.5	1°.0	1°.9	0.27 ± 0.07		–	–
2CG 054 + 01	3	54°.2	+1°.7	1°.0	1°.3	0.20 ± 0.09		–	–
2CG 065 + 00	4	65°.7	0°.0	0°.8	1°.2	0.24 ± 0.09		CG 64 + 0	–
2CG 075 + 00	5	75°.0	0°.0	1°.0	1°.3	–	could be an	CG 75 – 0	–
2CG 078 + 01	5	78°.0	+1°.5	1°.0	2°.5	–	extended feature	CG 78 + 1	–
2CG 095 + 04	3	95°.5	+4°.2	1°.5	1°.1	–		–	–
2CG 121 + 04	3	121°.0	+4°.0	1°.0	1°.0	0.43 ± 0.12		CG 121 + 3	–
2CG 135 + 01	3	135°.0	+1°.5	1°.0	1°.0	0.31 ± 0.10		CG 135 + 1	–
2CG 184 – 05	4	184°.5	−5°.8	0°.4	3°.7	0.18 ± 0.04		CG 185 – 5	–
2CG 195 + 04	3	195°.1	+4°.5*	0°.4	4°.8	0.33 ± 0.04	γ195 + 5	CG 195 – 4	–
2CG 218 – 00	3	218°.5	−0°.5	1°.3	1°.0	0.30 ± 0.08		–	–
2CG 235 – 01	2	235°.5	−1°.0	1°.5	1°.0	–		–	–
2CG 263 – 02	4	263°.6	−2°.5	0°.3	13°.2	0.36 ± 0.02		CG 263 – 2	PSR 0833–45
2CG 284 – 00	1	284°.3	−0°.5	1°.0	2°.7	–	could be an	–	–
2CG 288 – 00	1	288°.3	−0°.7	1°.3	1°.6	–	extended feature	–	–
2CG 289 + 64	2	289°.3	+64°.6	0°.8	0°.6	0.15 ± 0.07		CG 291 + 65	3C 273
2CG 311 – 01	2	311°.5	−1°.3	1°.0	2°.1	–		CG 312 – 1	–
2CG 333 + 01	3	333°.5	+1°.0	1°.0	3°.8	–		CG 33 + 0	–
2CG 342 – 02	5	342°.9	−2°.5	1°.0	2°.0	0.36 ± 0.09		–	–
2CG 353 + 16	4	353°.3	+16°.0	1°.5	1°.1	0.24 ± 0.09		–	ρOph
2CG 356 + 00	1	356°.5	+0°.3	1°.0	2°.6	0.46 ± 0.12	prob. variable	–	–
2CG 359 – 00	3	359°.5	−0°.7	1°.0	1°.8	–		–	–

[a] Assuming E^{-2} spectra.
[b] Intensity ($E > 300$ MeV)/Intensity ($E > 100$ MeV), assuming E^{-2} spectra calculating both intensities.
* See text.

describes the method, the performed Monte-Carlo simulations and experimental results (including data on the average extent of the published sources).

Based on the data acquired during the first $2\frac{1}{2}$ years of observation time the second COS-B catalogue of gamma-ray sources has been compiled (Swanenburg *et al.*, 1981; Hermsen, 1980) and is shown in Table I. It is noted that, although the sources in the Carina region (2CG 284 – 00 and 2CG 288 – 00) and in the Cygnus region (2CG 075 + 00 and 2CG 078 + 01) are quoted in the catalogue as individual entries, the corresponding structures could also be interpreted as extended features. Also, it has been recognized that the flux from the Cygnus region shows differences between several observations of this region, suggesting a contribution from variable sources, not related to Cyg X-3 (Bloemen *et al.*, 1981). One probably variable source (2CG 356 + 00) is contained in the catalogue. This source has been clearly seen only in one of four observations and presents a hint for time variability at the 99% confidence level.

After publication of the 2CG catalogue the position of one source has been updated, namely that of 2CG 195 + 04. New data became available on this source and the updated position is $l = 195.1°$, $b = 4.2°$ with an error radius of 0.4° (Masnou *et al.*, 1981; see also Figure 9).

The four identified sources in the catalogue have been discussed already in Section 2. Strictly taken, the source 2CG 353 + 16, identified with ρOph, should be deleted from the catalogue. Using more data than was available at the time of compilation of the catalogue, the source is now resolved (see Section 2.3). All remaining sources have been the subject of searches for counterparts measured at other wavelengths. Some have been studied in great depths. (e.g. 2CG 135 + 01 and 2CG 195 + 04; see the review by Bignami and Hermsen, 1983). Still, 21 sources lack firm identification.

3.2. Average properties of the unidentified gamma-ray sources

The vast majority of gamma-ray sources is galactic, as is evident from their distribution over the sky. In fact, 20 unidentified sources are closely aligned with the galactic-disc line emission. Most discussions on the nature of the unidentified sources are concentrated on these low-latitude sources. We do the same here.

Prime characteristics of a source are total luminosity and size. The lack of identification, and hence the lack of individual distances, prohibits the direct derivation of these parameters from the observations. In order to enable us to estimate the order of magnitude of these parameters we assume that all unidentified sources, or at least the majority, belong to one class of objects or population. With this assumption the main characteristics of this population follow from the observed longitude and latitude distribution (Swanenburg *et al.*, 1981). The average properties are summarized in Table II. Many other authors have discussed this topic (see e.g. Bignami and Hermsen, 1983, and reference therein). Among them Buccheri *et al.* (1981), who propose that the 2 kpc lower limit to the average distance is probably a 'typical' distance. This would imply that the typical luminosity of the 2CG sources is about 4×10^{35} erg s^{-1}, while they consider 2×10^{36} erg s^{-1} to be an upperlimit. These values would support their

TABLE II

Average properties of the unidentified galactic gamma-ray sources

Average $\|b\|$	$\sim 1.5°$
Angular size	$0° - 2°$
Photon-flux range (100 MeV $< E <$ 1 GeV)	$\sim (1–5) \times 10^{-6}$ ph cm^{-2} s^{-1}
Distance range	2–7 kpc
Scale height $\langle \|z\| \rangle$ ($300° < l < 60°$)	$\lesssim 130$ pc
Spectral shape	different for individual objects, average $dN/dE \sim E^{-2}$
Average photon energy	~ 250 MeV in the 100 MeV–1 GeV range
Energy-flux range (100 MeV $< E <$ 1 GeV)	$\sim (4–20) \times 10^{-10}$ erg cm^{-2} s^{-1}
Luminosity range (100 MeV $< E <$ 1 GeV)	$\sim (0.4–5) \times 10^{36}$ erg s^{-1}

suggestion that young (yet undetected) radio pulsars are the counterparts for most of the unidentified gamma-ray sources.

The proposed identification of the unidentified gamma-ray sources with radio pulsars is one of the many suggestions made to solve the problem of the puzzling nature of the sources. This is an example of a comparison between different populations of sources, using the average characteristics of the populations. Other attempts are made for individual sources by making detailed experimental investigations of the region of the sky covered by the COS-B error box. This way we derive constraints on source models which try to explain the emission from an individual source. An example is given below for 2CG 195 + 04 (Geminga). Also, many authors propose first theoretical scenario's for gamma-ray production which can then be tested against the experimental constraints or can stimulate the search for a particular object or astrophysical setting in the general direction of a gamma-ray source. In the introduction it was already noted, that a general discussion of these topics is beyond the scope of this paper. The reader is referred to the many papers on this topic in this volume and e.g. the review by Bignami and Hermsen (1983).

3.3. 2CG 195 + 04 (GEMINGA)

The source 2CG 195 + 04 was discovered by the SAS-2 experiment (Kniffen *et al.*, 1975) and called $\gamma 195 + 5$. In Figure 9 the SAS-2 error box (Thompson *et al.*, 1977) is indicated in a contour map of the gamma-ray intensities measured by COS-B for energies in the range 500 MeV to 5 GeV. The data are from four COS-B observations of typically 5 weeks duration each, between August 1975 and October 1980. The high-energy range is selected in order to exploit the best possible angular resolution obtainable with COS-B. A sharp source profile, representing ~ 190 counts, is nicely located in the SAS-2 error box (actually, the intrinsic source profiel has been smoothed to produce the contour map). The COS-B position is indicated in the figure, together with its uncertainty (Masnou *et al.*, 1981). The feature at $l \simeq 185°$, $b \simeq 6°$ is the Crab gamma-ray source; the position of PSR 0531 + 21 is indicated.

This unidentified gamma-ray source Geminga is a mystery, still 8 years after its discovery! Its gamma-ray spectrum is vastly different from that of Crab or Vela. In

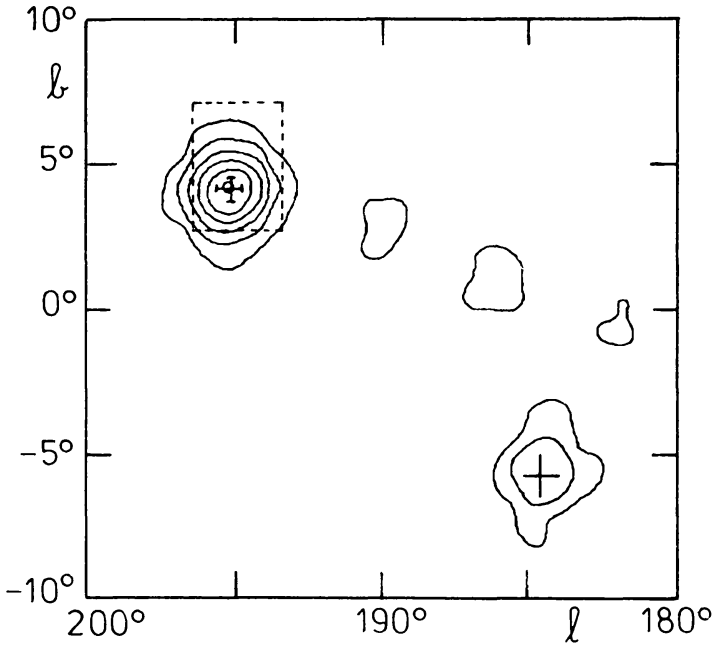

Fig. 9. Contour map of the gamma-ray intensities measured by COS-B for energies between 500 MeV and 5 GeV of the sky region containing Geminga and Crab. The COS-B exposure used to produce this map is for both sources $\sim 1.8 \times 10^8$ cm^2 s. The dotted lines indicate the SAS-2 error box for $\gamma 195 + 5$. Also is indicated the COS-B position with its uncertainty and the position of PSR 531 + 21.

Figure 9 it is evident that the strength of the source for energies between 500 MeV and 5 GeV is twice the strength of the total Crab, while at energies between 50 MeV and 100 MeV Geminga reaches only half the strength of the Crab pulsar! Sofar no unambiguous counterpart has been proposed for this enigmatic source; Bignami and Hermsen (1983) present a résumé of the experimental status in the search for counterparts, summarized in Figure 10. However, a recent and very tempting identification has been proposed by Bignami *et al.* (1983) after a deep survey of the Geminga error box in several wavelengths bands. Caraveo (1981) reported already on the discovery of an Einstein soft-X-ray source in the Geminga error box. This source (1 E0630 + 178) turned out to be a unique object. The detailed work by Bignami *et al.* (1983) resulted in the following expose: An identification was obtained with a faint blue object exhibiting a unique luminosity ratio $L_X/L_V \simeq 1300$, while no source has been found at 6 cm down to ~ 1 mJy using the VLA. The X-ray source (flux $\sim 2 \times 10^{12}$ erg cm^{-2} s^{-1}) has a very soft spectrum and little evidence has been found for interstellar absorption, leading to a distance estimate of 100 pc or less. Although no temporal evidence for the presence of a pulsar has been found, Bignami *et al.* (1983) argue that the extreme parameters characterizing this source, point at the presence of a neutron star.

Figure 10 shows the total energy spectrum from the radio range up to the ultra-high-energy gamma rays. The data point indicated at X-ray energies and the upper limit in the radio range, are drawn with the assumption that 1 E0630 + 178 is to be associated with the gamma-ray one. However, if the radio flat-spectrum source of which the

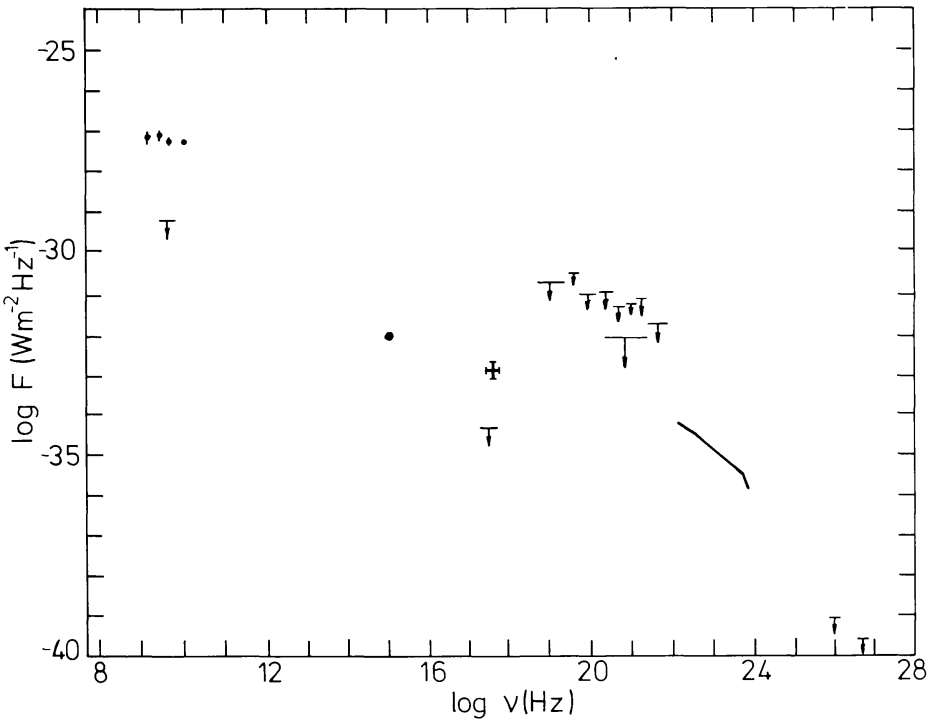

Fig. 10. Composition of spectral data for 2CG 195 + 04 (Geminga), drawn in the assumptions: (1) that the newly discovered X-ray source is to be associated with the gamma-ray one, (2) that the radio flat-spectrum source is the counterpart (see text). Data origins: see Bignami and Hermsen (1983).

spectrum is given in the figure, is the counterpart (as was suggested by Sieber and Schlickeiser, 1982), the upper limit at soft X-ray energies should be regarded. This latter suggestion is now less likely to be the reality, given the very interesting identification of 1 E0630 + 178. The COS-B gamma-ray spectrum is taken from Masnou *et al.* (1981).

Geminga is certainly the prototype of the unidentified gamma-ray sources. The energy flux (F) emitted by this source in the gamma-ray domain dominates the energy output in all other frequency bands by several orders of magnitude, e.g.: (1) if the radio flat-spectrum source is the counterpart, $\nu F_\gamma / \nu F_{\text{radio}} \approx 2 \times 10^5$ and $\nu F_\gamma / \nu F_x > 10^4$; and (2) if the Einstein X-ray source is the counterpart, $\nu F_\gamma / \nu F_{\text{radio}} > 10^7$ and $\nu F_\gamma / \nu F_x \approx 3 \times 10^3$. Most likely the mystery around the Geminga gamma-ray source has been solved now with the identification of the unique X-ray source 1 E0630 + 178.

Acknowledgements

The results presented in this paper are obtained, thanks to the continuing efforts of many colleagues in the Caravane Collaboration for the COS-B satellite. I thank Hans Bloemen for reading the manuscript and for some valuable contributions to this paper.

Appendix: Search for Point Sources

In the search for point sources in the COS-B data we used a cross-correlation method. The main advantage of such a method is that the presence in the data of the signature

of a point source, i.e. the point-spread function (PSF), is exploited, yielding a favourable combination of sensitivity, positional accuracy, and low susceptibility to spurious effects. On the other hand, the method imposes certain limitations. For instance, the effective angular resolution is slightly degraded, which impacts on the ability to distinguish between a real point source and an extended region of emission and on the sensitivity in confused regions. Also, if a candidate source is superimposed on a structured background, the excess should be fitted. This fitting procedure itself is not unique, but introduces a certain amount of interpretation. Therefore it is usefull to get insight in the applied method and to see examples from the data. What follows is an extended abstract from the presentation by Hermsen (1980) of the method and the data, with some additional figures and remarks.

A. Cross-correlation function

In looking for point sources we are examining the data for statistically significant excesses above the surrounding background, the excess having a spatial distribution consistent with the PSF. Therefore we search for a signal of predictable shape superimposed on the background. The general method available for separating signal and background in such a case is the cross-correlation method. With this method the distribution of the photon arrival directions is correlated with the PSF. A gamma-ray source is thus defined as an excess for which the cross-correlation analysis results in a significant positive correlation. From the amount of correlation also the strength of the source can be derived, or in case of lack of correlation an upper limit to the source strength.

We explain now the basis and the technical execution of this method. The data in the skymaps are grouped in skybins (D_{ij}) and may be presented in counts (N_{ij}) or in flux values (F_{ij}). The indexes i and j represent the bin coordinates in the skymap. When position $\mathbf{r}$ is taken as a trial position, the PSF, $f(\mathbf{r}, i, j)$, predicts the contribution of a source at $\mathbf{r}$ to bin (i, j). The correlation function $C(\mathbf{r})$ is then defined as

$$C(\mathbf{r}) = \frac{A}{m} \sum_{ij} (D_{ij} - \bar{D})(f(\mathbf{r}, i, j) - \bar{f}) , \tag{1}$$

where A is a normalization constant, yet to be chosen, m is the number of bins over which Σ_{ij} is accumulated, $\bar{D}$ is the average of D_{ij} and $\bar{f}$ is the average of $f(\mathbf{r}, i, j)$ over the area of the m bins considered. In the computations square arrays containing m bins are used. The distribution of $C(\mathbf{r})$ over the skymap is called the correlation map. If for a point $\mathbf{r}$ the deviations of D_{ij} with respect to $\bar{D}$ have predominantly the same sign as the deviation of $f(\mathbf{r}, i, j)$ with respect to $\bar{f}$, $C(\mathbf{r})$ is positive. We would like to underline the importance of the inclusion in this correlation function of the average values $\bar{D}$ and $\bar{f}$. The result is, that structures with angular sizes lager than the PSF are partly suppressed, while a uniform background, or a background linear with r, gives even zero correlation. A source superimposed on such a background causes non zero correlations as a function of $\mathbf{r}$.

Equation (1) may be rewritten in the form

$$C(\mathbf{r}) = A\left[\frac{\Sigma fD}{m} - \frac{(\Sigma f)(\Sigma D)}{m^2}\right], \tag{2}$$

where all subscripts are omitted for clarity. The normalization constant A can be chosen in such a way that, if we take for D_{ij} the number of counts

$$N_{ij} = \frac{N_s}{\Sigma' f} f(\mathbf{r}, i, j) + B\,, \tag{3}$$

where B is a uniform background level, N_s is the total number of counts (= strength) of the source, and $\Sigma' f$ is the sum over the total PSF, the maximum value of the correlation function equals the source strength. This gives

$$C_n(\mathbf{r}) = [m\,\Sigma fN - (\Sigma f)(\Sigma N)]\,\frac{\Sigma' f}{m\,\Sigma f^2 - (\Sigma f)^2}\,. \tag{4}$$

Similarly, if we take the flux values F_{ij} instead of the number of counts:

$$C_f(\mathbf{r}) = [m\,\Sigma fF - (\Sigma f)(\Sigma F)]\,\frac{\Sigma' f}{m\,\Sigma f^2 - (\Sigma f)^2}\,. \tag{5}$$

In principle the correlation functions may be determined for *any* point in a skymap by accumulating the sums over the *entire* map.

For practical reasons three restrictions are made:

(i) Sky bins of size $0.5 \times 0.5°$ are used.

(ii) The correlation function is determined only at the centre of bins. This is justified because a step size of $0.5°$ is fine enough in view of the available statistics.

(iii) The sums are accumulated over a smaller array, usually a matrix of about $10° \times 10°$ or $15° \times 15°$. This is done to restrict the range over which significant structure (e.g. strong source, or galactic plane) affects the value of the correlation.

Examples of the response of the cross-correlation analysis to a strong point source (PSR 0833 – 45, Vela) are given in Figure 11. The derived correlation maps peak at the position of the pulsar and it is verified that the correct number of source counts is retrieved by using the PSF as determined by the pre-launch calibration. The negative 'ring' around the maximum reflects the expected anti-correlation.

B. Probability Density Function

A good insight into the statistical behaviour of the cross-correlation function is essential, both for estimating the accuracy of intensities and positions, and even more so for deriving firm conclusions about the statistical significance of the results. Therefore, Hermsen (1980) determined the probability density function (PDF) of the cross-correlation function. The shape of the PDF depends on the used PSF, the number of counts in the matrix and the matrix size. For the COS-B profile and counting statistics the

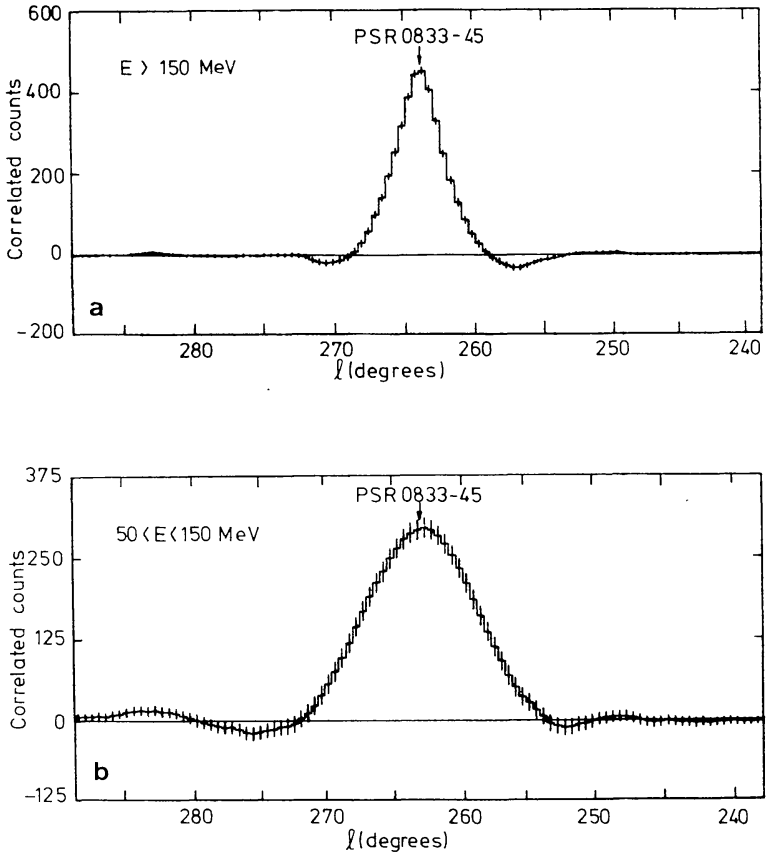

Fig. 11. Longitude profiles across PSR 0833−45 in the correlation map for (a) energies above 150 MeV and (b) energies between 50 MeV and 150 MeV. In both figures the diffuse galactic gamma-ray background is suppressed because the events are selected in the peaks of the light curve of the pulsar.

cross-correlation function does not follow Gaussian statistics. Two examples of the PDF are shown in Figure 12 for parameters typical for COS-B high-latitude observations and the energy range $E > 150$ MeV. The peak at negative values of C (or C_n) and the tail towards positive values are apparent. For a field without sources (flat background, high-latitude observations) the parent mean is 0 and the parent standard deviation of the distribution of values for C found, is given by

$$\sigma_0(C) = \frac{1}{m^2}\sqrt{(m\,\Sigma f^2 - (\Sigma f)^2)\Sigma N}\,, \tag{6}$$

where again the subscripts are deleted.

The ratio

$$C/\sigma_0 = \frac{m(\Sigma fN) - (\Sigma f)(\Sigma N)}{\sqrt{(m\,\Sigma f^2 - (\Sigma f)^2)\Sigma N}} \tag{7}$$

gives the correlation value in number of parent standard deviations for a random distribution of the counts. A sufficiently large value of C/σ_0 indicates that the data set probably does *not* represent a random distribution of counts, possibly indicating the

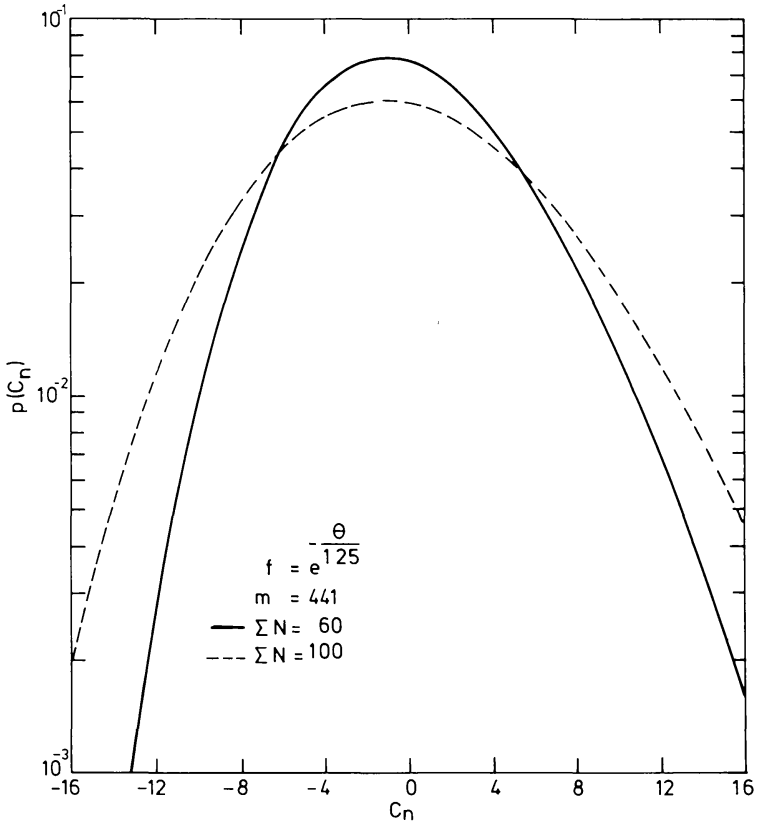

Fig. 12. Two probability density functions of the cross-correlation function for different ΣN as a function of C_n (Equation (4)) for the energy range $E > 150$ MeV. The point-spread function, f, applicable in this energy range is given.

presence of a source. The probability can be worked out numerically, as was done to produce Figure 12. For large ΣN the PDF may be approximated by the normal distribution.

If the values of C/σ_0 indicate that we do have a significant correlation, we claim the detection of a source with strength given by (4) (correlated counts) or (5) (correlated flux). Then we wish to attribute a variance to the correlation (or source strength) actually measured. For this we have to derive the sample variance of the measured C or C_n. These are respectively (Hermsen, 1980):

$$\sigma(C) = \frac{1}{m^2}\sqrt{[m^2\,\Sigma\,(f^2N) + (\Sigma f)^2\,\Sigma N - 2m(\Sigma f)(\Sigma fN)]}\,, \tag{8}$$

$$\sigma(C_n) = \sigma(C)\,\frac{m^2\,\Sigma f}{m\,\Sigma f^2 - (\Sigma f)^2}\,. \tag{9}$$

C. Monte Carlo simulations

Although the PDF of the cross-correlation function can be determined numerically and the response of the correlation analysis to fine structure in the data can be calculated,

representative simulations of complicated situations encountered in the flight data, including the effect of a non-uniform background, are needed. Expecially near the Galactic Centre the background is in the form of a strong line source and systematically yields a positive correlation. Another aspect which can only be assessed by simulations is the evaluation of the probability to detect spurious sources as a result of a *search* for sources by analysing points of maximum correlation. The significance of each maximum is reduced because in the search a large number of trials is made, namely one for each bin in the correlation map. Therefore, the probability to find a maximum of given significance anywhere in the map is proportional to the number of *independent* trials. By the nature of the correlation function a certain degree of correlation exists between individual trials. The derivation of the degree of correlation of individual bins in the correlation map cannot be done analytically. Therefore simulations are needed.

In the case of a uniform background region (applicable in the COS-B data for high-latitude observations) the simulation is unambiguous and a sufficiently accurate approximation for the probability calculation is determined (Hermsen, 1980). A probability threshold, of finding a value C_n or larger, of $< 10^{-5}$ is adopted in the flight data analysis. With this threshold the probability of accepting a spurious source in a single high latitude observation is $\sim 3\%$.

The situation is more complex if the candidate source is superimposed on a structured background, because the expectation value of C is not zero in this case. This situation occurs in the flight data along the galactic plane for $|b| < 5°$, where the line source introduces a positive excess in the correlation map. Figure 13 presents a one-dimensional

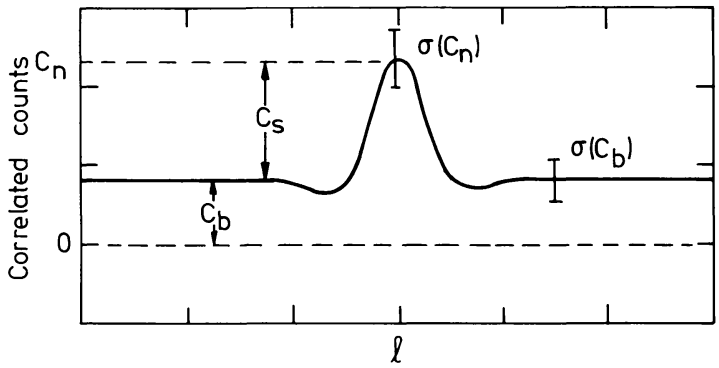

Fig. 13. One-dimensional sketch of a correlation map for a source superimposed on a line source. Explanation is given in the text.

sketch of such a situation, i.e. a point source superimposed on a line source which is parallel to the longitude direction. The values of C_n and $\sigma(C_n)$ at the source position are not a measure of the correlation and significance of the source, but of the combination of source *and* background (i.e. the line source). In Figure 13 the number of counts attributed to the source is C_s and to the background C_b. The values of C_s and C_b are derived using a fitting procedure. Since no independent background estimate is available (still at least for the major fraction of the galactic plane region), each candidate source is fitted and subtracted, in such a manner that the remaining background connects

smoothly with the surroundings. The fitted source strength (C_s) together with the parameters $\sigma(C_n)$ and ΣN at the fitted position are then used to express the significance of the excess in number of standard deviations (σ_0') of the underlying background (Hermsen, 1980). Since it cannot be assumed that the statistical behaviour of the values obtained by the fit is identical to that of the correlation values in the single bins, and because the fitting procedure itself is not unique but introduces a certain amount of interpretation, the entire method is calibrated by analysing representative simulated skymaps. This calibration also removes the ambiguity resulting from the unknown number of independent trials made in a search.

Because the shape and strength of the galactic gamma-ray distribution varies with longitude, nine longitude intervals, each 10° wide, are selected to give a representative sample of plane shapes (in latitude direction), plane to background ratios and counting statistics. In total 99 skymaps, 40° wide in longitude each, are simulated, namely 11 for each latitude distribution. No structure as a function of longitude is introduced in the simulation. The correlation maps have been analysed in the latitude range $|b| < 5°$. The entire search thus covers 1.584×10^5 bins of size $0.5° \times 0.5°$, equivalent to a surface 11 times the measured galactic plane distribution in the same latitude range. Candidate (spurious) sources are fitted and judged by eye using an interactive computer display terminal, identical to the procedure followed for the flight-data analysis. The significance in C_s/σ_0' is calculated for each analysed excess. The number of counts in the region along the galactic plane is high. Therefore, Gaussian statistics are initially assumed to apply and the corresponding probability for random occurence for the analysed excess is calculated. The results from the simulations show that the proposed calculation of the significance (Gaussian statistics) gives a save upper limit for the expected numer of random excesses as a function of probability (Hermsen, 1980). Therefore, in the flight data analysis of the structured region $|b| < 5°$ a probability threshold of 10^{-6} ($\sim 4.75\sigma_0'$) is adopted, so that for $|b| < 5°$ (i.e. 1.44×10^4 bins) the probability to accept a spurious source is $< 2\%$.

D. Results

In Section 3, the 2CG catalogue of high-energy ($E > 100$ MeV) gamma-ray sources has been introduced and the average properties of the sources have been discussed. Below, the appearances in the data of several sources contained in the catalogue are shown in order to give a good impression of the actual measurements.

Most results obtained for high-latitude regions are shown already: 2CG 353 + 16, now being resolved and unambiguously identified with ρOph (Section 2.3) and 2CG 289 + 64 or 3C 273 (Section 2.4). One more source is detected away from the galactic plane: 2CG 010−31. It is measured at about the significance level obtained for 3C 273 in a single observation: $5.7\sigma_0$ for 33 counts, giving $P(C_n) = 4.6 \times 10^{-8}$. Confirmation is needed in this case.

The search for sources along the galactic plane encounters two main problems: (i) sources are superimposed on a structured background, (ii) source confusion occurs due to a high surface density of possible sources.

In the region of the plane $50° \lesssim l \lesssim 310°$ source confusion is minimal. Here, this problem mainly plays a role in the Cygnus and the Carina region. For both cases two sources are contained in the catalogue: the measured distributions are best explained with the presence of these sources, but it cannot be excluded that they are part of more extended features (as is stated in the catalogue). For other regions in this longitude interval confusion doesnot play an important role. Therefore, selection of data with the best possible angular resolution, namely for energies above 300 MeV or 500 MeV, is not required. All reported sources are detected for energies above 100 MeV or 150 MeV. Figure 14a, 14b, and 14c show examples of the profile of a gamma-ray source in the

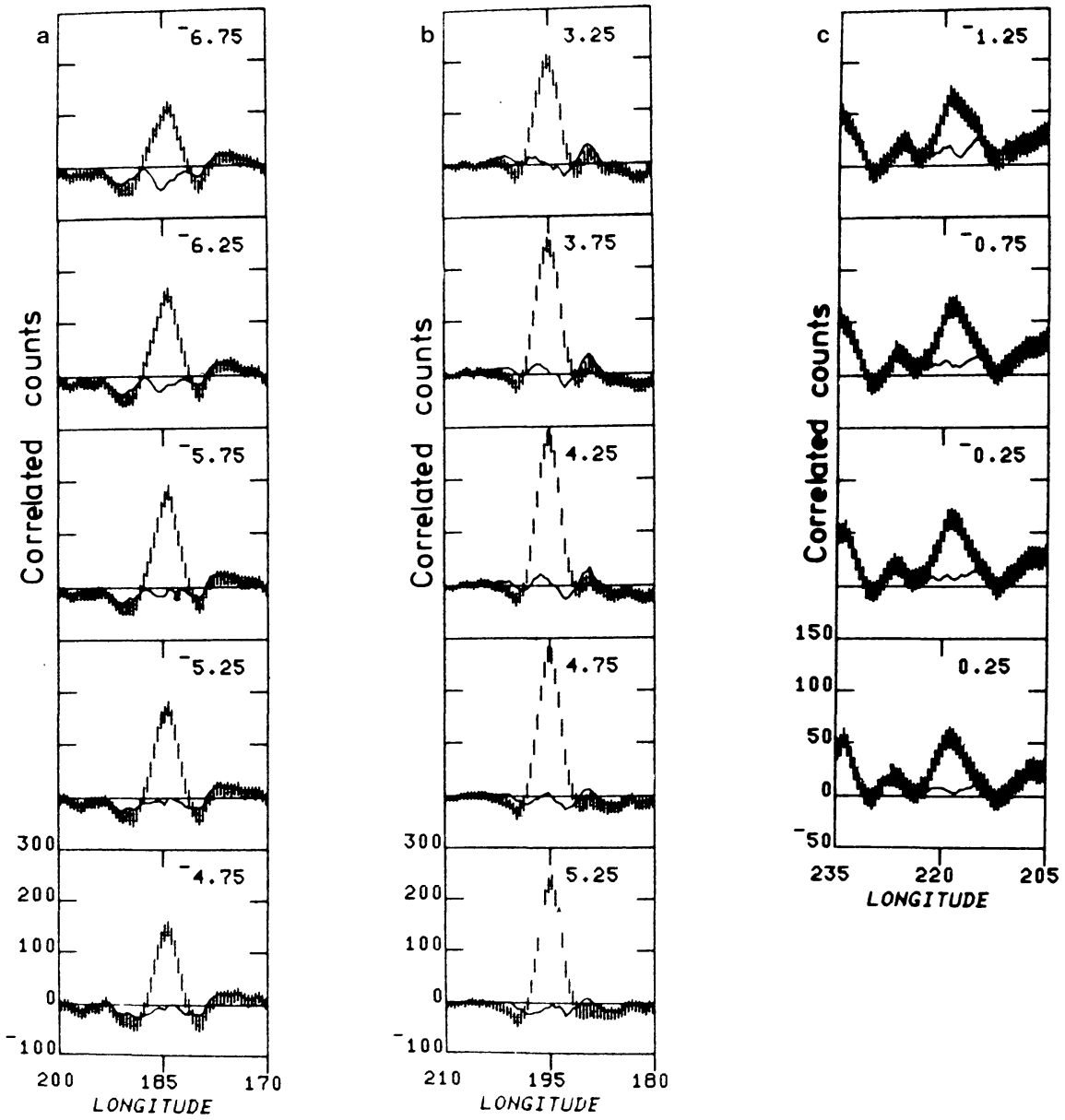

Fig. 14. Longitude profiles of the correlation maps showing for energies above 150 MeV (a) 2CG 184 – 05 (Crab), (b) 2CG 195 + 04 (Geminga), and for energies above 100 MeV (c) 2CG 218 – 00. The latitude values are given for each profile. The solid lines show the distributions which remain after subtraction of the cross-correlated point-spread functions at the positions of the sources.

correlation map for: (a) a genuine point source (PSR 0531 + 21, Crab, 2CG 184 – 05; $E > 150$ MeV), (b) a strong unidentified source (Geminga, 2CG 195 + 04; $E > 150$ MeV), and (c) a weak unidentified source (2CG 218 – 00; $E > 100$ MeV). In each figure the solid line shows the distribution which remains after subtraction of the cross-correlated PSF at the position of the source. Evidently, all three excesses have a shape compatible with the PSF. Hardly any plane component is evident in the correlation maps, except in the case of 2CG 218 – 00, for which a relatively small positive correlation remains after subtraction of the source profile. This can be quite different in other regions, such as that around 2CG 135 + 01. Figure 15a presents, for energies above 100 MeV, the correlation map containing this source and 2CG 121 + 04. The source feature representing 2CG 135 + 01 is superimposed on a positive structured, background correlation of at least the same strength as that of the source. When one tries to relate the reported flux of 2CG 135 + 01 to the total mass of the clouds in the general direction of the source, this positive background correlation should be explained by part of that total mass as well. This has been ignored by Issa and Wolfendale (1981)

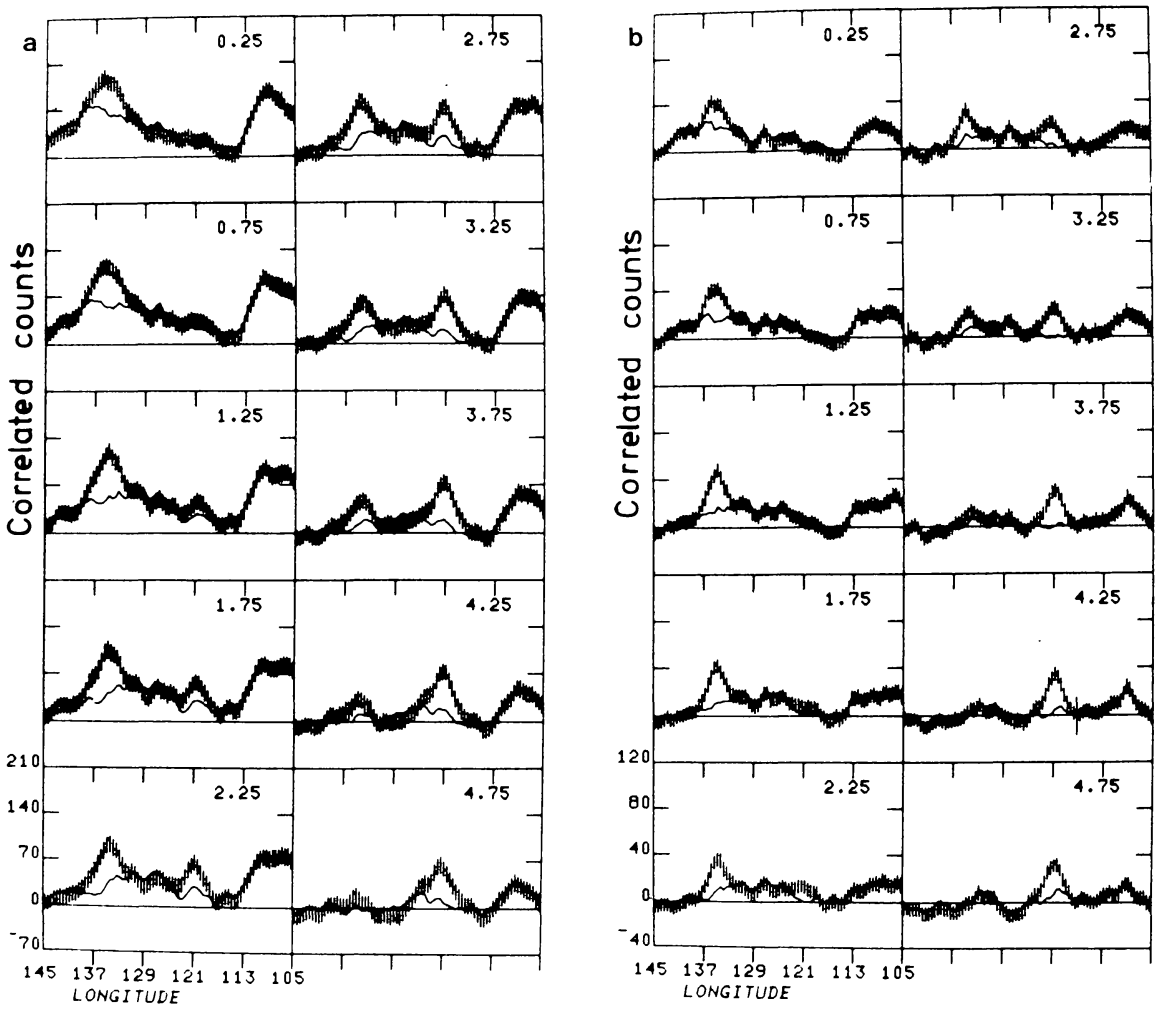

Fig. 15. Longitude profiles of the correlation maps showing 2CG 135 + 01 and 2CG 121 + 04 for energies above (a) 100 MeV and (b) 300 MeV. See legend of Figure 14.

in the case of this source and several others. The source 2CG 121 + 04 is well away from the plane, therefore, the background level is lower. Both sources show up nicer in Figure 15b for energies above 300 MeV. The background level in the correlation map is practically reduced to zero at the position of 2CG 121 + 04 and is also reduced relative to the source strength for 2CG 135 + 01. In addition the profiles are sharper.

In the longitude interval encompassing the direction of the Galactic Centre, $310° \lesssim l \lesssim 50°$, source confusion dominates in the integral energy range above 100 MeV. Given the COS-B PSF, counting statistics and applied selection criteria it is practically impossible to resolve source features from the general galactic structure at a sufficiently high significance level. In fact, all sources reported in the 2CG catalogue

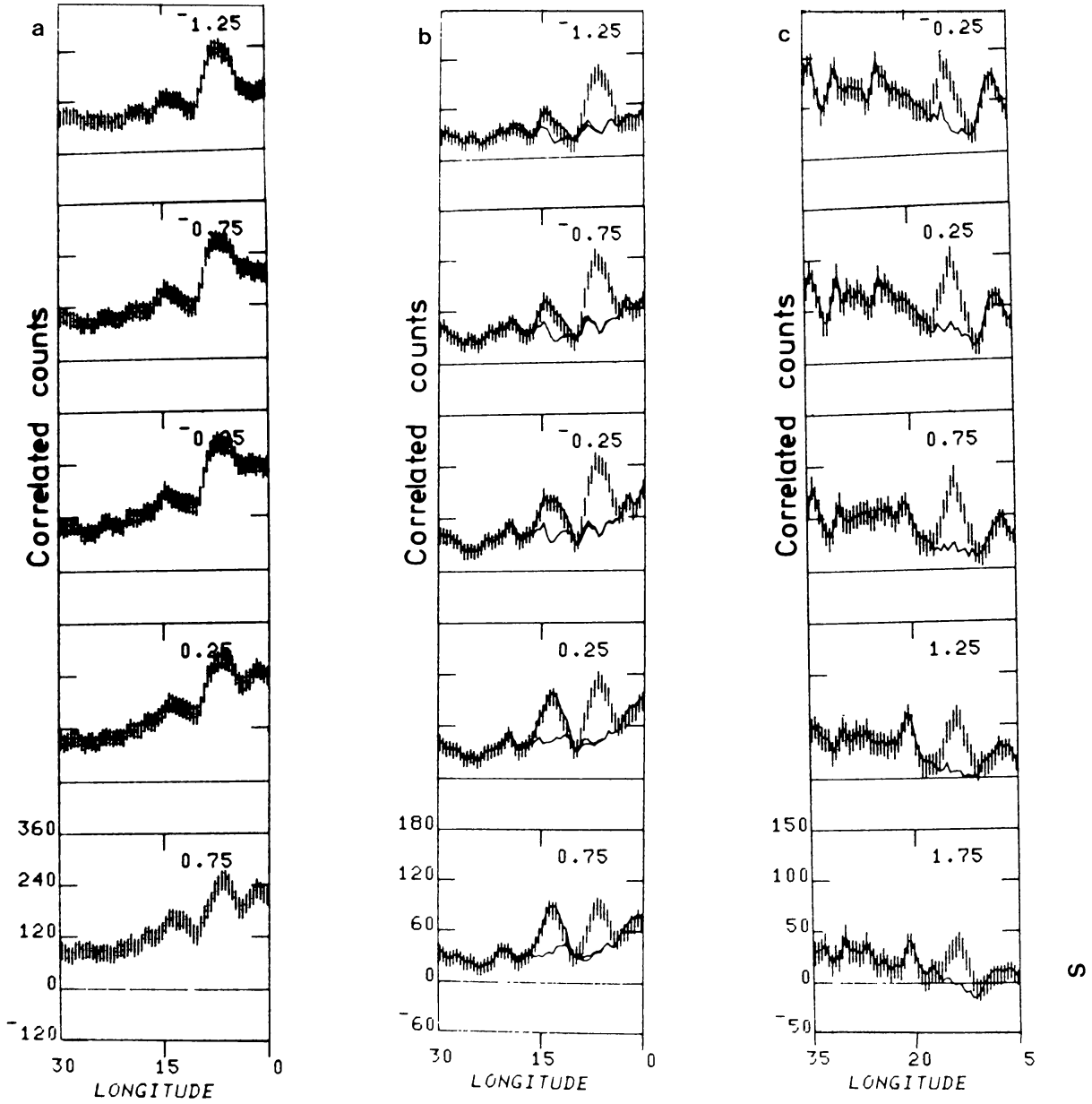

Fig. 16. Longitude profiles of the correlation maps showing the region containing 2CG 006 − 00 and 2CG 013 + 00 for energies above (a) 100 MeV, (b) 300 MeV, and (c) 500 MeV. See legend of Figure 14.

which are located within this longitude interval are detected at energies above 300 MeV (seven sources), with the single exception of 2CG 311 + 01 (detected for $E > 150$ MeV), which is located just at the boundary of this interval and of the intense ridge of gamma radiation from the inner Galaxy. The following examples are representative for the confusion problem in this longitude range. First two examples from the data base used to compile the 2CG catalogue. Figures 16a, 16b, and 16c present the gamma-ray sources 2CG 006 – 00 and 2CG 013 + 00 in the correlation map. For all energies above 100 MeV (Figure 16a) practically all information is lost on the fine structure, in particular no evidence at all can be claimed for a source at $l = 13.7, b = 0.6$ (2CG 013 + 00). However, the source feature of 2CG 006 – 00 can easily be resolved at energies above 300 MeV (Figure 16b). In fact, also a significant correlation is found for 2CG 013 + 00 in this energy range. The sharp feature, consistent with the PSF, for energies above 500 MeV (Figure 16c), leaves no doubt on the presence of an excess at $l = 13.7$, $b = 0.6$. (For significance levels, observation periods used, etc., see Hermsen, 1980.) These sources are shown two dimensionally in Figures 17 and 18 for energies above 100 MeV and

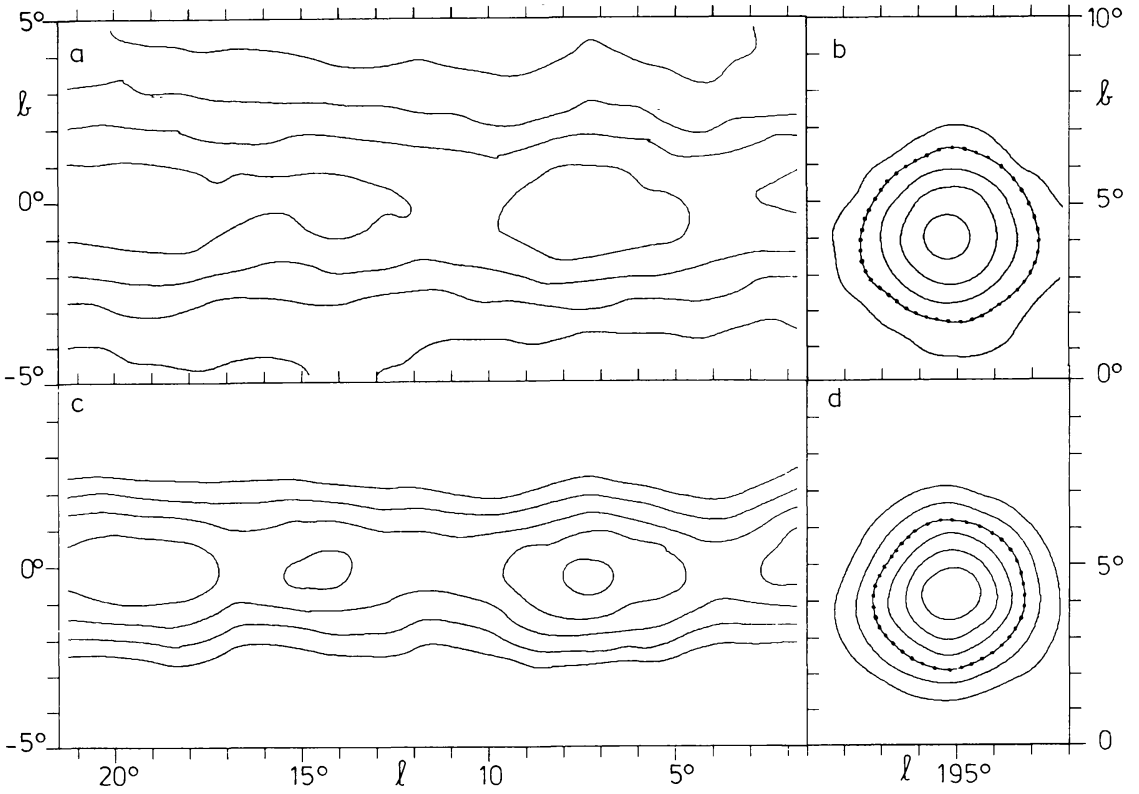

Fig. 17. Contour maps ($E > 100$ MeV) of two very different regions of the sky: (a) and (c) containing 2CG 006 – 00, 2CG 013 + 00 and the strong galactic 'line' source; (b) and (d) containing 2CG 195 + 04 (Geminga) and effectively no background emission. (a) intensity map; contour levels are indicated at 3.0, 4.5, 6 and 7.5×10^{-4} photon $cm^{-2} s^{-1} sr^{-1}$. (b) intensity map; contour levels at 2, 3, 4, 5, and 6×10^{-4} photon $cm^{-2} s^{-1} sr^{-1}$. (c) correlation map (correlated flux); contour levels at multiples of 6×10^{-7} photon $cm^{-2} s^{-1}$. (d) correlation map (correlated flux); contour levels at multiples of 5×10^{-7} photon $cm^{-2} s^{-1}$. The dotted contour levels in (b) and (d) indicate the level of ~45% of the peak value of the source profiles. Evidently, no feature of the same angular extent in latitude and exhibiting closed contour lines, is present in (a) or (c).

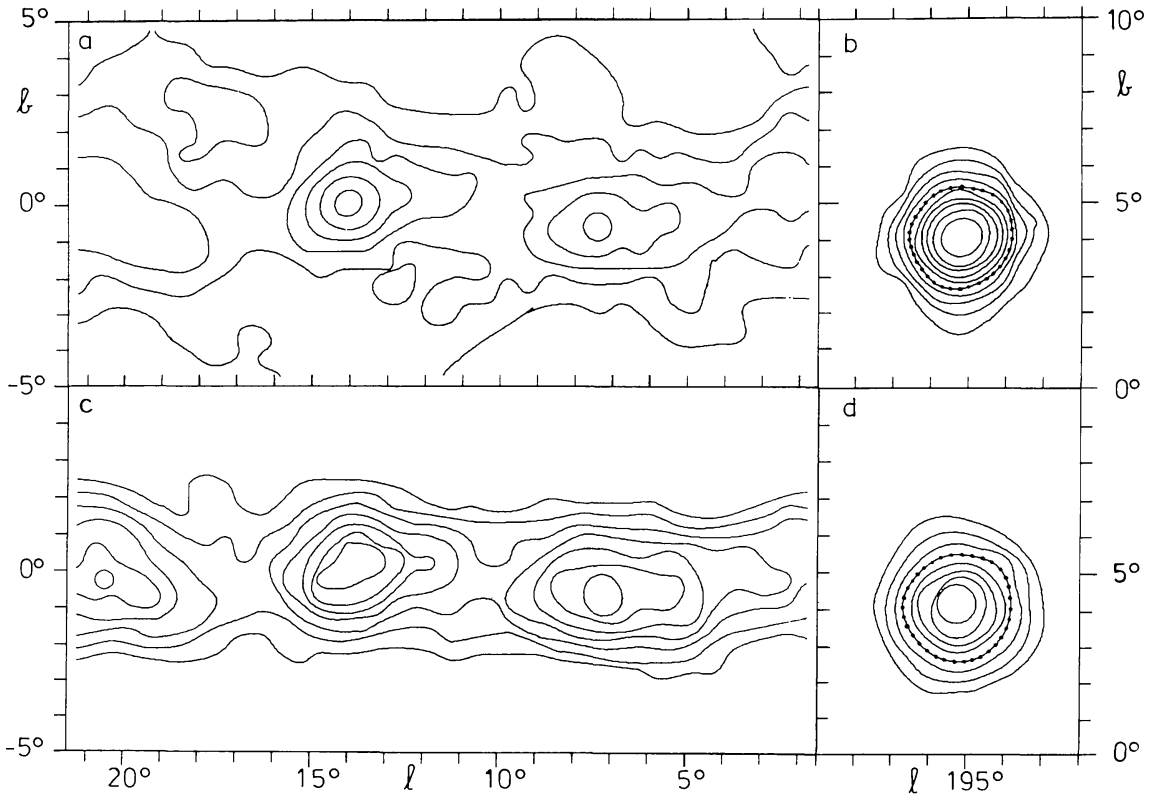

Fig. 18. Contour maps like the ones shown in Figure 17 but for $E > 500$ MeV. Contour levels are indicated at multiples of: (a) 5×10^{-5} photon $cm^{-2}\,s^{-1}\,sr^{-1}$, (b) 2.5×10^{-5} photon $cm^{-2}\,s^{-1}\,sr^{-1}$ with the first contour at 5×10^{-5} photon $cm^{-2}\,s^{-1}\,sr^{-1}$, (c) 1×10^{-7} photon $cm^{-2}\,s^{-1}$, and (d) 1×10^{-7} photon $cm^{-2}\,s^{-1}\,sr^{-1}$ with the first contour at 2×10^{-7} photon $cm^{-2}\,s^{-1}$.

500 MeV, respectively (some additional data are used to produce these figures). For both energy ranges contour maps are given for intensity maps (a), correlated-flux maps (c), and the corresponding maps showing the Geminga source feature for comparison (b) and (d). Again it is evident that in the maps for energies above 100 MeV no source feature can be resolved. At energies above 500 MeV the fine structure is apparent with source features near to $b = 0°$ (the shapes of the sources are somewhat elongated due to the underlying line source).

Li and Wolfendale (1982) discuss the nature of the gamma-ray sources and claim that the majority of the catalogued sources are 'apparent sources' due to the irradiation of clumpy interstellar medium by cosmic ray electrons and nuclei. This conclusion is reached from a Monte Carlo analysis for the longitude interval $10° < l < 100°$. For that interval they predict the gamma-ray intensity distribution for energies above 100 MeV starting from the available information on the distribution of gas (CO and H I data) and using the assumption of a uniform cosmic-ray distribution. Furthermore, they claim that the characteristics of the COS-B detector are imposed in the Monte Carlo analysis as well as the finite number of gamma-ray counts detected experimentally, and, finally, that the COS-B technique of source identification is adopted. However, in their five simulations of the gamma-ray distribution for energies above 100 MeV, they 'detect' at

least 4 out of 5 times a gamma-ray source at $l \simeq 12°$, $l \simeq 25°$, $l \simeq 38°$, $l \simeq 49°$, $l \simeq 79°$, and $l \simeq 93°$. In all these cases it is in the actual flight data impossible to resolve source features for the integral energy range above 100 MeV (see e.g. in Figure 17 the case of 2CG 013 + 00, which Li and Wolfendale 'detected' in every simulation and therefore classified as an 'apparent source'). Therefore it is evident that their combination of (subjective) fitting procedure and acceptance criteria is *not* representative for the analysis actually applied to the COS-B flight data. As a result, one may conclude that there is no sound basis to apply their significance calculations to the 2CG sources and no conclusions are allowed to be drawn on the nature of the sources. Also their reference to an analysis of SAS-2 data (Houston and Wolfendale, 1982) is ambiguous, since: (1) the binning of the SAS-2 data ($2.5° \times 0.8°$) results in an effectively even worse angular resolution, (2) the low SAS-2 exposure of the sky makes the analyses impossible (taking into account the ratio of the SAS-2 exposure to the COS-B exposure used to compile the 2CG catalogue, on average ~ 8 counts per source are expected in the SAS-2 data), (3) no fits to the correlation maps are made like was done in the COS-B analysis, (4) errors were made in the calculation of the probability values of the claimed effects (A. W. Wolfendale, private communication).

The gamma-ray sources contained in the 2CG catalogue are present in the data as *statistically significant* excesses above the surrounding background. *All* excesses have a spatial distribution consistent with the PSF. This means that the lower limit which can be set on the angular extent for *each* source is 0°. The high lower limits claimed for some of the sources by Li and Wolfendale (1981) are not in agreement with the experimental data (all reported sources *do* fit the PSF) nor is the claimed high accuracy on the derived extent for some sources (e.g. $6.3° \pm 1.6°$ for 2CG 218 – 00, which is shown in Figure 14c to fit nicely the PSF). The average extent of the sources has been claimed by Hermsen (1980) to be less than 1° to 2°. Li and Wolfendale (1981) tried to fit published COS-B data (by Hermsen, 1980) and arrived at values of $\sim 4°$ (the diameter of an equivalent sphere of uniform volume emissivity). In order to give an impression of the most likely average extent the following procedure has been worked out: For the region along the Galactic plane (containing 22 sources) skymaps in the energy range 300 MeV to 5 GeV are produced, such that in each skymap a source is placed in the central bin. High-energy data is selected since the better angular resolution enables a more accurate determination of the angular extent. Then, a point-summation technique is applied, namely, all skymaps are summed to obtain one total map with the total source signal again in the central bin. Finally the total correlation map is produced. Excluded from the analysis are the 'pair sources' in the Cygnus and Carina regions, to avoid confusion. In addition the three strongest sources, the genuine point sources PSR 0833 – 45 and PSR 0531 + 21 and Geminga, are also excluded. The first two, because their angular extent is known, the latter, because its large number of counts would dominate the result. Of the 15 sources which remain, no source contributes more than 10% to the total number of counts. Like in the analysis of Li and Wolfendale, a geometrically simple source model has been assumed: spheres of uniform volume emissivity. The total source feature, shown in Figure 19a, is fitted with the correlation profiles for source diameters (D) of

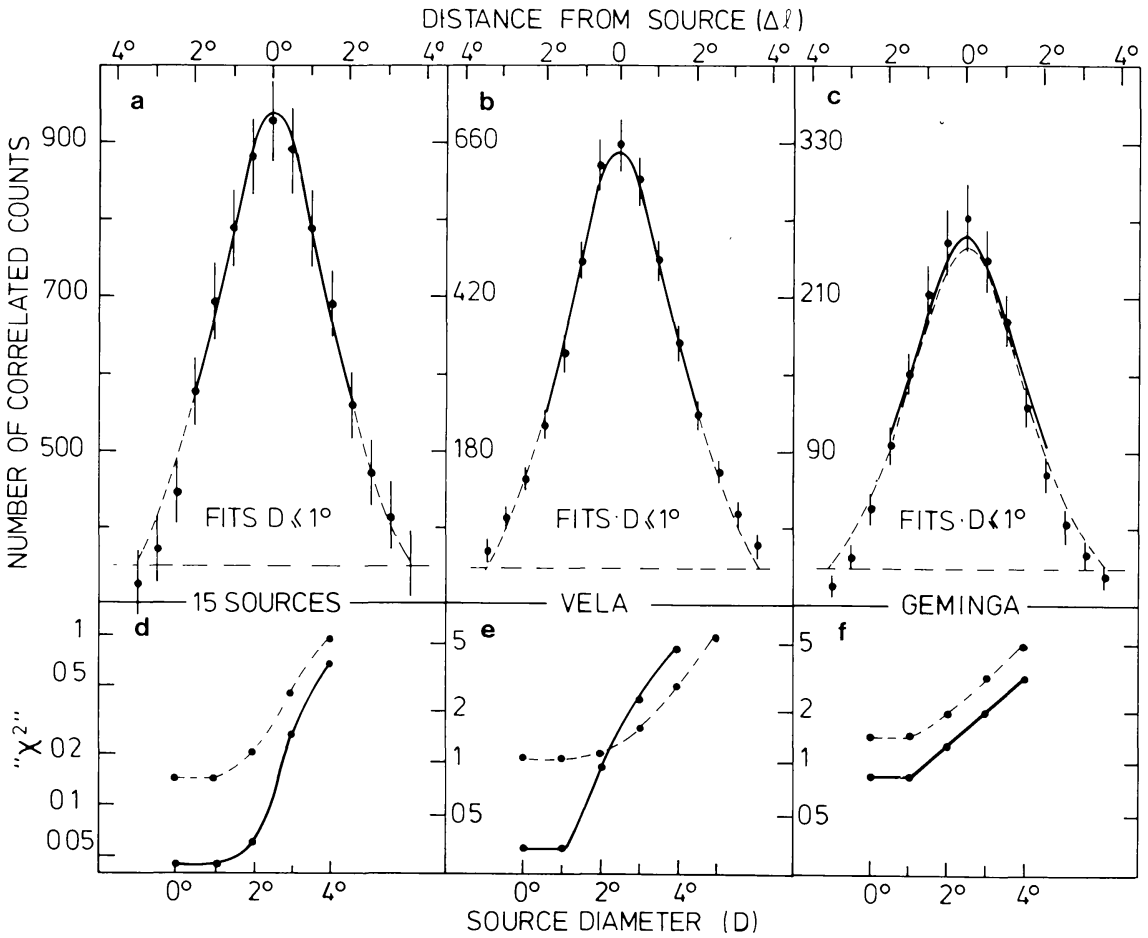

Fig. 19. The upper figures show longitude profiles of the correlation maps across the position of (a) the maximum of the summed profiles of 15 2CG sources (see text), (b) Vela, and (c) Geminga (2CG 195 + 04). The lower figures present the dependence of the minimum, reduced χ^2 values on source diameter (see text). The solid lines give the results obtained for fits to 9 points of the correlation profile, the broken lines for fits to 15 data points.

0° up to 4° and 'χ^2' values are calculated to judge the fits. Since the values in Figure 19a are not independent for each bin, it is not possible to calculate directly a probability for the goodness of fit. However, one obtains a valid indication for the most-probable average angular extent. The best fit to the data points is indicated in Figure 19a and the obtained χ^2 values are given as a function of D in Figure 19d. The whole excercise has been performed also for PSR 0833 – 45, to show the appearance of a genuine point source, and for Geminga being a strong unidentified source (Figure 19b, c, e, f). It is evident that the three cases shown, are quite similar. One should note that the uncertainties in the source positions will broaden the distribution of the total summed signal somewhat. In the case of Geminga the number of counts is significantly lower than for PSR 0833 – 45. The conclusion from these figures is that the average extent of the sources is indeed between 0° and 2°. As far as the individual sources are concerned: some of the weak sources and sources detected only in the integral energy range above 100 MeV certainly have a higher *upper limit* to the angular extent. However, as remarked upon before, for all sources the lower limit to D remains 0°. Still, in the search for

counterparts of the gamma-ray sources, the indicated average extent of the sources does not a priori rule out molecular clouds, bombarded by high-energy cosmic rays, to be the counterparts of some individual sources. Therefore, if a dense gas cloud (or more than one) is detected in the direction of a gamma-ray source a detailed comparison should be made, between the total gamma-ray emission from that direction and the available astronomical data.

References

Bennett, K., Bignami, G. F., Boella, G., Buccheri, R., Hermsen, W., Kanbach, G., Lichti, G. G., Masnou, J. L., Mayer-Hasselwander, H. A., Paul, J. A., Scarsi, L., Swanenburg, B. N., Taylor, B. G., and Wills, R. D.: 1977a, *Astron. Astrophys.* **61**, 279.

Bennett, K., Bignami, G. F., Hermsen, W., Mayer-Hasselwander, H. A., Paul, J. A., and Scarsi, L.: 1977b, *Astron. Astrophys.* **59**, 273.

Bignami, G. F. and Hermsen, W.: 1983, *Ann. Rev. Astron. Astrophys.* **21**, 67.

Bignami, G. F. and Morfill, G. E.: 1980, *Astron. Astrophys.* **87**, 85.

Bignami, G. F., Boella, G., Burger, J. J., Keirle, P., Mayer-Hasselwander, H. A., Paul, J. A., Pfefferman, E., Scarsi, L., Swanenburg, B. N., Taylor, B. G., Voges, W., and Wills, R. D.: 1975, *Space Sci. Instr.* **1**, 245.

Bignami, G. F., Bennett, K., Buccheri, R., Caraveo, R., Hermsen, W., Kanbach, G., Lichti, G. G., Masnou, J. L., Mayer-Hasselwander, H. A., Paul, J. A., Sacco, B., Scarsi, L., Swanenburg, B. N., and Wills, R. D.: 1981, *Astron. Astrophys.* **93**, 71.

Bignami, G. F., Caraveo, P. A., and Lamb, R. C.: 1983, *Astrophys. J. Letters*, in press.

Black, J. H. and Fazio, G. G.: 1973, *Astrophys. J. Letters* **185**, L7.

Bloemen, J. B. G. M.: 1983, in W. L. H. Shuter (ed.), *Kinematics, Dynamics and Structure of the Milky Way*, D. Reidel Publ. Co., Dordrecht, Holland, p. 31.

Bloemen, J. B. G. M., Bennett, K., Caraveo, P. A., Hermsen, W., Kanbach, G., Masnou, J. L., Mayer-Hasselwander, H. A., Paul, J. A., Sacco, B., Strong, A. W., and Wills, R. D.: 1981, *Proc. 17th Int. Cosmic Ray Conf. Paris* **1**, 181.

Buccheri, R.: 1981, in W. Sieber and R. Wielebinski (eds.) 'Pulsars', *IAU Symp.* **95**, 241.

Buccheri, R.: 1983, *Bull. Am. Astron. Soc.* **14** (4), 966.

Buccheri, R., Morini, M., and Sacco, B.: 1981, *Phil. Trans. Roy. Soc. London* **A301**, 495.

Buccheri, R., Bennett, K., Bignami, G. F., Bloemen, J. B. G. M., Boriakoff, V., Caraveo, P. A., Hermsen, W., Kanbach, G., Manchester, R. N., Masnou, J. L., Mayer-Hasselwander, H. A., Özel, M. E., Paul, J. A., Sacco, B., Scarsi, L., and Strong, A. W.: 1983, *Astron. Astrophys.*, in press.

Caraveo, P. A.: 1981, *Phil. Trans. Roy. Soc. London* **A301**, 523.

Caraveo, P. A., Bennett, K., Bignami, G. F., Hermsen, W., Kanbach, G., Lebrun, F., Masnou, J. L., Mayer-Hasselwander, H. A., Paul, J. A., Sacco, B., Scarsi, L., Strong, A. W., Swanenburg, B. N., and Wills, R. D.: 1980, *Astron. Astrophys.* **91**, L3.

Caraveo, P. A., Barbareschi, L., Bennett, K., Bignami, G. F., Hermsen, W., Kanbach, G., Lebrun, F., Masnou, J. L., Mayer-Hasselwander, H. A., Sacco, B., Strong, A. W., and Wills, R. D.: 1981, *Proc. 17th Int. Cosmic Ray Conf., Paris* **1**, 139.

Danaher, S., Fegan, D. J., Porter, N. A., and Weekes, T. C.: 1981, *Nature* **289**, 568.

Fazio, G. G.: 1973, in H. Bradt and R. Giacconi (eds.), *X- and Gamma-Ray Astronomy*, D. Reidel Publ. Co., Dordrecht, Holland, p. 303.

Galper, A. M., Kirillov-Ugryumov, V. G., Kurochkin, A. V., Leikov, P. G., Luchkov, B. I., and Yurkin, Yu. T.: 1976, *Pisma v. Astron. Zh.* **2**, 254.

Galper, A. M., Kirillov-Ugryumov, V. G., Kurochkin, A. V., Leikov, P. G., Luchkov, B. I., Yurkin, Yu. T., Fomin, V. P., Neshpor, Yu. I., Stepanian, A. A., and Vladimirsky, B. M.: 1977, *Proc. 15th Int. Cosmic Ray Conf., Plovdiv* **1**, 131.

Gregory, P. C., Kronberg, P. P., Seaquist, E. R., Hughes, V. A., Woadsworth, A., Viner, M. R., and Retallack, D.: 1972, *Nature* **239**, 440.

Hermsen, W.: 1980, 'Gamma-Ray Sources', Ph.D. Thesis Univ. of Leiden, Holland.

Hermsen, W.: 1981, *Phil. Trans. Roy Soc. London* **A301**, 519.

Hermsen, W. and Bloemen, J. B. G. M.: 1983, in W. B. Burton and F. P. Israel (eds.), *Proc. Leiden Workshop on Southern Galactic Surveys*, D. Reidel Publ. Co., Dordrecht, Holland, in press.

Hermsen, W., Swanenburg, B. N., Bignami, G. F., Boella, G., Buccheri, R., Scarsi, L., Kanbach, G., Mayer-Hasselwander, H. A., Masnou, J. L., Paul, J. A., Bennett, K., Higdon, J. C., Lichti, G. G., Taylor, B. G., and Wills, R. D.: 1977a, *Nature* **269**, 494.

Hermsen, W., Bennett, K., Bignami, G. F., Boella, G., Buccheri, R., Higdon, J. C., Kanbach, G., Lichti, G. G., Masnou, J. L., Mayer-Hasselwander, H. A., Paul, J. A., Scarsi, L., Swanenburg, B. N., Taylor, B. G., and Wills, R. D.: 1977b, in R. D. Wills and B. Battrick (eds.), *Recent Advances in Gamma-Ray Astronomy*, ESA SP-124, p. 13.

Hermsen, W., Bennett, K., Bignami, G. F., Bloemen, J. B. G. M., Buccheri, R., Caraveo, P. A., Kanbach, G., Masnou, J. L., and Wills, R. D.: 1981, *Proc. 17th Int. Cosmic Ray Conf., Paris* **1**, 230.

Houston, B. and Wolfendale, A. W.: 1982, *Proc. Roy Irish Acad.*, in press.

Issa, M. R. and Wolfendale, A. W.: *Nature* **292**, 430.

Kanbach, G., Bennett, K., Bignami, G. F., Buccheri, R., Caraveo, P., D'Amico, N., Hermsen, W., Lichti, G. G., Masnou, J. L., Mayer-Hasselwander, H. A., Paul, J. A., Sacco, B., Swanenburg, B. N., and Wills, R. D.: 1980, *Astron. Astrophys.* **90**, 163.

Khavtassi, J. Sh.: 1960, *Atlas of Galactic Dark Nebulae*, Tiblis, Abastumani Astrophys. Obs.

Kniffen, D. A., Hartman, R. C., Thompson, D. J., Bignami, G. F., Fichtel, C. E., Tümer, T., and Ögelman, H.: 1974, *Nature* **25**, 397.

Kniffen, D. A., Bignami, G. F., Fichtel, C. E., Hartman, R. C., Ögelman, H., Thompson, D. J., Özel, M. E., and Tümer, T.: 1975, *Proc. 14th Int. Cosmic Ray Conf. Munchen* **1**, 100.

Lamb, R. C., Fichtel, C. E., Hartman, R. C., Kniffen, D. A., and Thompson, D. J.: 1977, *Astrophys. J. Letters* **212**, L63.

Lamb, R. C., Godfrey, C. P., Wheaton, W. A., and Tümer, T.: 1982, *Nature* **296**, 543.

Li, T. P. and Wolfendale, A. W.: 1981, *Astron. Astrophys.* **100**, L26.

Li, T. P. and Wolfendale, A. W.: 1982, *Astron. Astrophys.* **116**, 95.

Lichti, G. G., Buccheri, R., Caraveo, P., Gerardi, G., Hermsen, W., Kanbach, G., Masnou, J. L., Mayer-Hasselwander, H. A., Paul, J. A., Swanenburg, B. N., and Wills, R. D.: 1980, in R. Cowsik and R. D. Wills (eds.), *Non-Solar Gamma Rays (COSPAR)*, Advances in Space Exploration, Vol. 7, p. 49, Pergamon Press, Oxford and New York.

Manchester, R. N. and Taylor, J. H.:1977, *Pulsars*, Freeman Publ. Co., San Francisco, U.S.A.

Masnou, J. L., Bennett, K., Bignami, G. F., Bloemen, J. B. G. M., Buccheri, R., Caraveo, P. A., Hermsen, W., Kanbach, G., Mayer-Hasselwander, H., Paul, J. A., and Wills, R. D.: 1981, *Proc. 17th Int. Cosmic Ray Conf. Paris* **1**, 177.

Mayer-Hasselwander, H. A., Bennett, K., Bignami, G. F., Buccheri, R., D'Amico, N., Hermsen, W., Kanbach, G., Lebrun, F., Lichti, G. G., Masnou, J. L., Paul, J. A., Pinkau, K., Scarsi, L., Swanenburg, B. N., and Wills, R. D.: 1980, *Ann. NY Acad. Sci.* **336**, 211.

Meegan, C. A. and Fishman, G. J.: 1979, *Astrophys. J. Letters* **234**, L123.

Mukanov, J. B., Nesterova, N. M., Stepanian, A. A., and Fomin, V. P.: 1979, *Proc. 16th Int. Cosmic Ray Conf., Kyoto* **1**, 143.

Neshpor, Yu. I., Stepanian, A. A., Fomin, V. P., Gerasimov, S. A., Vladimirsky, B. M., and Ziskin, Yu. L.: 1979, *Astrophys. Space Sci.* **61**, 349.

Parsignault, D., Gursky, H., Kellog, E., Matilsky, T., Murray, S., Schreier, E., Tananbaum, H., Giacconi, R., and Brinkman, A.: 1972, *Nat. Phys. Sci.* **239**, 129.

Samorksi, M. and Stamm, W.: 1983, *Astroph. J. Letters*, in press.

Scarsi, L., Bennett, K., Bignami, G. F., Boella, G., Buccheri, R., Hermsen, W., Koch, L., Mayer-Hasselwander, H. A., Paul, J. A., Pfeffermann, E., Stiglitz, R., Swanenburg, B. N., Taylor, B. G., and Wills, R. D.: 1977, in R. D. Wills and B. Battrick (eds.), *Recent Advances in Gamma-Ray Astronomy*, ESA SP-124, p. 3.

Sieber, W. and Schlickeiser, R.: 1982, *Astron. Astrophys.* **113**, 314.

Swanenburg, B. N., Bennett, K., Bignami, G. F., Caraveo, P., Hermsen, W., Kanbach, G., Masnou, J. L., Mayer-Hasselwander, H. A., Paul, J. A., Sacco, B., Scarsi, L., and Wills, R. D.: 1978, *Nature* **275**, 298.

Swanenburg, B. N., Bennett, K., Bignami, G. F., Buccheri, R., Caraveo, P., Hermsen, W., Kanbach, G., Lichti, G. G., Masnou, J. L., Mayer-Hasselwander, H. A., Paul, J. A., Sacco, B., Scarsi, L., and Wills, R. D.: 1981, *Astrophys. J. Letters* **243**, L69.

Thompson, D. J., Fichtel, C. E., Kniffen, D. A., and Ögelman, H. B.: 1975, *Astrophys. J. Letters* **200**, L79.

Thompson, D. J., Fichtel, C. E., Hartman, R. C., Kniffen, D. A., and Lamb, R. C.: 1977, *Astrophys. J.* **213**, 252.

Van der Klis, M. and Bonnet-Bidaud, J. M.: 1981, *Astron. Astrophys.* **95**, L5.

Weekes, T. C. and Helmken, H. F.: 1977, in R. D. Wills and B. Battrick (eds.), *Recent Advances in Gamma-Ray Astronomy*, ESA SP-124, p. 39.

Wills, R. D., Bennett, K., Bignami, G. F., Buccheri, R., Caraveo, P. A., Hermsen, W., Kanbach, G., Masnou, J. L., Mayer-Hasselwander, H. A., Paul, J. A., and Sacco, B.: 1981, *Proc. 17th Int. Cosmic Ray Conf. Paris* **1**, 22.

Wills, R. D., Bennett, K., Bignami, G. F., Buccheri, R., Caraveo, P. A., Hermsen, W., Kanbach, G., Masnou, J. L., Mayer-Hasselwander, H. A., Paul, J. A., and Sacco, B.: 1982, *Nature* **296**, 723.

Wouterloot, J. G. A.: 1981, 'The Large-Scale Structure of Molecular Clouds', Ph.D. Thesis Univ. of Leiden, Holland.